NREL/TP-451-4852 • NREL/TP--451-4852

DE92 010560

Fundamental Studies of Defect Generation in Amorphous Silicon Alloys Grown by Remote Plasma-Enhanced Chemical-Vapor Deposition (Remote PECVD)

Annual Subcontract Report 1 September 1990 - 31 August 1991

G. Lucovsky, R. J. Nemanich,
J. Bernholc, J. Whitten, C. Wang,
B. Davidson, M. Williams, D. Lee,
C. Bjorkman, Z. Jing
North Carolina State University
Raleigh, North Carolina

NREL technical monitor: J. Benner

National Renewable Energy Laboratory
(formerly the Solar Energy Research Institute)
1617 Cole Boulevard
Golden, Colorado 80401-3393
A Division of Midwest Research Institute
Operated for the U.S. Department of Energy
under Contract No. DE-AC02-83CH10093

Prepared under Subcontract No. XM-9-18141-2

January 1993

NOTICE

Printed in the United States of America
Available from:
National Technical Information Service
U.S. Department of Commerce
5285 Port Royal Road
Springfield, VA 22161

Price: Microfiche A01
Printed Copy A04

Codes are used for pricing all publications. The code is determined by the number of pages in the publication. Information pertaining to the pricing codes can be found in the current issue of the following publications which are generally available in most libraries: *Energy Research Abstracts (ERA)*; *Government Reports Announcements* and Index (*GRA* and I); *Scientific and Technical Abstract Reports (STAR)*; and publication NTIS-PR-360 available from NTIS at the above address.

Table of Contents

Summary of Major Research Accomplishments During Phase II

1. Deposition of Doped Hydrogenated Amorphous Silicon

We have demonstrated that the Remote PECVD process can be used to deposit heavily doped n-type and p-type a-Si:H thin films. Deposition is accomplished by pre-mixing the P-atom and B-atom source gases, PH_3 and B_2H_6, respectively, with SiH_4, and exciting these mixtures downstream with active species from a remote He plasma, primarily electrons with energies <10 eV. Using the same ratios of dopant atom source gases to SiH_4, the dark conductivities and activation energies of the most heavily doped Remote PECVD films are comparable to those of heavily doped films deposited by the conventional glow discharge, GD, process. In addition, the dark conductivity, and dark conductivity activation energy for heavily doped p-type a-Si:H are approximately the same for films deposited from 0.1 B_2H_6/SiH_4 with, and without molecular hydrogen at a downstream flow ratio of 30 with respect to SiH_4, and therefore 300 with respect to B_2H_6.

2. Deposition of Doped Microcrystalline Si (μc-Si) by Remote PECVD

We have optimized conditions for deposition of undoped, near-intrinsic and heavily-doped thin films of μc-Si by Remote PECVD. This is achieved at substrate temperature of 250°C, with an H_2/SiH_4 flow rate ratio of 30:1, and with the H_2 and the Si-atom and dopant atom source gases injected downstream from the plasma generation region. Conductivities of 50-100 S/cm for n-type material, and 6-10 S/cm for p-type μc-Si, with activations energies of 0.02 eV and 0.040 eV respectively, have been achieved for source gas mixtures of 10^{-2} PH_3/SiH_4 and 10^{-3} B_2H_6/SiH_4, respectively.

3. Deposition of a-Si,C:H and μc-Si,C Alloys by Remote PECVD

We have extended the Remote PECVD process to the deposition of undoped and doped a-Si,C:H and μc-Si,C alloy films. This has been accomplished by adding the carbon atom source gas, CH_4, downstream, along with the Si and dopant atom source gases, and for the case of μc-Si,C, also downstream injection of H_2. We have compared the dark conductivities of the a-Si,C:H and μc-Si,C alloy films, respectively, with those of a-Si:H and μc-Si, and have been shown that the decreased conductivity of the Si,C alloy films can be attributed to the wider band-gaps of the Si,C alloys. For

the case of the μc-Si,C films this means that the dark conductivities are limited by thermal emission of carriers from the Si crystallites into the a-Si,C:H material that separates the Si crystallites, and as such the dark conductivities in films with bandgaps of 2 eV or more are limited to values up about 0.1 S/cm.

4. Transport Mechanisms in Si and Si,C Amorphous and Microcrystalline Films

We have analyzed transport data for the dark conductivity in undoped and doped a-Si:H, a-Si,C:H, μc-Si and μc-Si,C films and have concluded that the transport in the microcrystalline films can be limited by two mechanisms: i) thermionic emission over energy barriers at the boundaries of the crystalline and amorphous regions; or ii) by thermal assisted tunnelling from the crystallites into band tail states of the amorphous component. Analysis of data in terms of these two mechanisms explains the relatively high dark conductivities that can be obtained in μc-Si, ~5-100 S/cm, and identifies a significant limitation on the attainment of conductivities higher than 0.1 S/cm in Si,C alloy films with bandgaps greater than about 2 eV.

5. Formation of Device Structures using Doped a-Si:H and μc-Si

We have studied the properties of doped a-Si:H and μc-Si in MOS capacitors using ~10 Ω-cm p-type crystalline substrates and thermally grown SiO_2 dielectric layers. These studies have provided information about the electron affinities of a-Si:H and μc-Si, and the effective Debye lengths in μc-Si films with different levels of p-type and n-type doping. This information is important in the design of solar cell structures that utilize the doped a-Si:H or doped μc-Si in the p- and n-layers of p-i-n structures.

6. Defect States in a-Si:H by Sub-Pico-Second Spectroscopies

We have collaborated with Professor Kurz's group at RWTH in Aachen, Germany, and have studied the contributions of process induced defect states to recombination of photogenerated electron-pairs. We find that the process induced defect states that contribute to the sub-bandgap absorption, as determined by CPM, also serve as recombination centers for an Auger type recombination process for electron-hole pairs that dominates in the sub-picosecond time regime.

7. Modelling of Bond and Dihedral Angle Disorder in a-Si:H

We have applied a tight-binding model to Si-Bethe lattice structures in order to investigate the effects of bond-angle, and/or dihedral angle disorder. We have used a Hamiltonian with nearest and second-nearest neighbor interactions, and have identified, and separated the effects bond angle disorder and dihedral angle disorder on the states at the conduction and valence band edges.

8. Chemical Effects in Local Bonding Arrangements in a-Si:H: Ab Initio and Empirical Calculations

We have used ab initio and empirical calculations to study non-random bonding arrangements in a-Si,O:H and doped a-Si:H films. The two approaches give comparable results for the bond energies of SiH groups that are near-neighbors to the oxygen and dopant atoms. The calculations have been used to develop a model for the way in which these bonding arrangements are created in thin film deposition processes in which surface, rather than gas phase reactions dominate; i.e., for the range of deposition parameters used to produce electronic or device grade materials.

I. Research Progress Report

The research milestones proposed for phase II include the following tasks as stated in the proposal for research, and the statement of work for this program.

Phase II

(a) Formation of p-i-n structures for PV studies.

(b) Defect generation by light-soaking in PV devices.

(c) Deposition of a-Si,C:H, μc-Si,C:H and a-Si,Ge:H alloy films.

(d) Fabrication of MOS/MIS structures: study of accumulation bias induced defects.

(e) Correlation between process modifications, and structural and spectroscopic properties of Remote PECVD a-Si:H films.

(f) Modelling of defect structures, including their properties and their introduction into the film growth process.

Significant progress has been made in most of these areas, with the milestone goals either being met, or sometimes exceeded. However, we have experienced problems in fabricating p-i-n device structures in our single chamber system. The most serious problems were related to development of chamber cleaning and/or conditioning procedures that would allow the deposition of the i-region materials. Consequently our progress in p-i-n fabrication was signifantly hampered. In addition, we had a serious equipment failure in the multichamber system that is has been used to fabricate a-Si TFT devices. This has delayed our activities for six months: tried to initially repair the process pump, and finally, had to find the funds to purchase a new pump. This system has just come back on line, and we are preparing to deposit TFT structures.

1. Deposition of Doped Hydrogenated Amorphous Silicon

We have demonstrated that the Remote PECVD process can be used to produce heavily doped n-type and p-type a-Si:H thin films. Deposition is accomplished by pre-mixing the P-atom and B-atom source gases, PH_3 and B_2H_6, respectively, with SiH_4, and exciting these mixtures downstream with active species from a remote He plasma, primarily electrons with energies <10 eV. The conductivities and activation energies of the most heavily doped films are comparable to those of doped films

deposited by the conventional glow discharge, GD, process using the same ratios of dopant atom source gases to SiH_4. In addition, the dark conductivity, and dark conductivity activation energy for heavily doped p-type a-Si:H, ~2-3x10^{-3} S/cm and ~0.3 eV, respectively, are the same for films deposited from 0.1 B_2H_6/SiH_4, with and without molecular hydrogen (30:1 ratio with respect to the SiH_4 flow) added to the source gas mixture. In contrast, and as discussed later on, the properties of doped a-Si,C:H films are altered significantly when a similar flow rate ratio of molecular hydrogen is introduced in these depositions.

The highest dark conductivities, and lowest dark conductivity activation energies achieved are listed in the table below, along with the properties of undoped a-Si:H films for reference:

Table 1.1: Electrical Properties of a-Si:H by Remote PECVD

Material	H_2/SiH_4 ratio	Dopant Gas/ SiH_4 ratio	Dark Conductivity (S/cm) = $(\Omega cm)^{-1}$	Activation Energy (eV)
a-Si:H	0	0	2.4 x 10^{-10}	0.80
a-Si:H(n)	0	1x10^{-2}	2.0 x 10^{-3}	0.25
a-Si:H(p)	0	1x10^{-1}	2.4 x 10^{-3}	0.31
a-Si:H(p)	30:1	1x10^{-2}	4.0 x 10^{-5}	0.40
a-Si:H(p)	30:1	1x10^{-1}	3.0 x 10^{-3}	0.30

The highest values of dark conductivity achieved in these studies are adequate for the fabrication of p-i-n device structures. We have verified that we could make p-i-n devices by combining depositions of the heavily doped p-type and n-type materials, with the deposition of an undoped i-layer. These devices showed significant rectification in the dark I-V characteristics, and exhibited modest photovoltages, but relatively high short-circuit currents (see results reported in first year-end report for this program).

2. Deposition of Dopend Microcrystalline Si (μc-Si) by Remote PECVD

We have optimized the conditions for deposition of undoped, near-intrinsic and heavily-doped thin films of μc-Si by Remote PECVD. This is achieved at substrate temperature of 250°C, with an H_2/SiH_4 flow rate of 30:1, and with the H_2 and the Si-atom and dopant atom source gases injected downstream from the plasma generation region. Conductivities of 50-100 S/cm for n-type material, and 6-10 S/cm for p-type μc-Si, with activations energies of 0.02 eV and 0.040 eV respectively, have been achieved for source gas mixtures of 10^{-2} PH_3/SiH_4 and 10^{-3} B_2H_6/SiH_4, respectively. The electrical properties of these films are displayed in Table 2.1.

From the table, we see that n-type μc-Si films have been grown from P-atom/Si-atom source gas mixtures up to and including 10^{-2} PH_3/SiH_4, whereas p-type μc-Si films could only be grown from B-atom/Si-atom source gas mixtures to 10^{-3} B_2H_6/SiH_4. Films deposited from B-atom/Si-atom source gas mixtures $>10^{-3}$ B_2H_6/SiH_4 were amorphous as determined from the Raman scattering spectrum, and from TEM imaging and electron diffraction.

TABLE 2.1: Electrical Properties of μc-Si Films by Remote PECVD

Material	H_2/SiH_4 ratio	Dopant Gas/ SiH_4 ratio	Dark Conductivity (S/cm) = $(\Omega cm)^{-1}$	Activation Energy (eV)
μc-Si	30:1	0	6.0×10^{-4}	0.30
μc-Si(N)	30:1	3×10^{-5}	0.2	0.08
μc-Si(N)	30:1	3×10^{-4}	5.0	0.05
μc-Si(N)	30:1	1×10^{-2}	40	0.018
μc-Si(P)	30:1	1×10^{-5}	6.0×10^{-8}	0.70
μc-Si(P)	30:1	2×10^{-4}	7.0×10^{-4}	0.24
μc-Si(P)	30:1	1×10^{-3}	6.0	0.04
a-Si:H(P)	30:1	1×10^{-2}	4.0×10^{-5}	0.40
a-Si:H(P)	30:1	1×10^{-1}	3.0×10^{-3}	0.30

We have conducted a detailed study of the most-resistive μc-Si, the films grown from the $B_2H_6/SiH_4 = 10^{-5}$ source gas mixture. These films are qualitatively different than the undoped films with regard to their photoconductivity, and have opened up what we believe to be interesting new options for device structures.

Boron-compensated μc-Si thins films were deposited using a 10^{-5} ratio of B_2H_6 to SiH_4[1-2]. These films displayed dark conductivities as low as 6.0×10^{-8} S/cm with activation energies up to 0.66 eV. These films also have a relatively high photoconductivity, ~10^{-4} S/cm to ~0.5 AM1 white light. The E_{04} band gap was approximately 1.4 eV, as determined by the photon energy at which the absorption constant is 10^4 cm^{-1}. Measurements of the photoconductivity of this B-compensated μc-Si under prolonged light exposure indicated no photodegradation for soaking times up to 40 hours at light levels of ~0.5 AM1[2].

The dark conductivity of the μc-Si material changes from n-type to B-compensated-intrinsic, and eventually to strongly p-type over a narrow range of B_2H_6 to SiH_4 doping mixtures[3]. *Exact* compensation was difficult to achieve and depended on the recent deposition history of the chamber, which had also been used to deposit n- and p-type Si and Si,C materials. Attempts to minimize chamber contamination have had only limited success[3]. One aspect of this study examined data from films deposited under identical conditions, but influenced by residual B-doping, and possible P-compensation derived from the chamber walls and fixtures. In this way we have generated a series of B-compensated μc-Si films that display a range of electrical properties that span the region in which exact numerical compensation can occur.

The dark conductivity at 300K as a function of the dark conductivity activation energy for a series of these films can be fit to an expression, $\sigma = \sigma_0^* \exp (- E_\sigma^*/kT_{eff})$, with $\sigma_0^* = 5.0 \pm 5$ S/cm, and $T_{eff} = 400K \pm 30K$. The significance of the fit parameters has been discussed in detail elsewhere[4,5]: i) the activation energy, E_σ^* represents an internal barrier between the Si crystallites and the intervening a-Si:H material; ii) σ_0^* is the band conductivity in the extended states of the a-Si:H; and iii) T_{eff} is an effective temperature that includes the *effects* of the Meyer-Neldel relationship between σ_0^* and E_σ^*. A value of T_{eff} greater than the measurement temperature means that the energy, E_0, in the Meyer-Neldel relationship $\sigma_0^* = C \exp (E_\sigma^*/E_0)$, is positive[4], in this instance, approximately 0.12 eV.

Figure 2.1(a) displays conductivity and photo-conductivity vs E_σ^* for B-doped μc-Si. These data show a weak dependence of the photo-conductivity, to 0.5 AM1 white-light exposure, on the dark conductivity activation energy. As the E_σ^* increases, the photoconductivity decreases by a relatively small amount compared to the decrease in the dark conductivity for the same change in E_σ^*. There is an inherent ambiguity in these data plotted as a function of the activation energy that derives from the behavior of the conductivity versus doping curves. The conductivity initially drops in the defect-controlled region as diborane is introduced into the source gas mixture. It reaches a minimum when the B-atoms *exactly compensate* the donor-like defects, and then increases again as the material becomes p-type. The *same values* of the dark conductivity and the activation energy can then occur on *both sides* of the conductivity minimum. Specifically, the activation energy first *increases* in the defect-controlled region, and then *decreases* after compensation is exceeded and the material becomes p-type. In order to develop an understanding of the dark conductivity and photoconductivity behaviors on both sides of the compensation point, we have obtained the B-concentrations, [B], on a subset of these films using SIMS, and have replotted the conductivity data in terms of this variable, [B], in Fig. 2.1(b).

From the variation of dark conductivity with [B] in Fig. 2.1(b), we observe that the film with the lowest B concentration, ~$3x10^{17}$ cm^{-3}, is an n-type film, in which the native defects have not been completed compensated. The sample with the lowest conductivity and highest activation energy with a B concentration of ~$5x10^{17}$ cm^{-3} is close to *intrinsic*; in the context of an exact compensation of native defects by active boron acceptors. The two samples with B-atom concentrations of 1 and $2x10^{18}$ cm^{-3}, are p-type, and the activation energy is relative to the valence band. The dark conductivity varies by almost four orders of magnitude as the B-concentration increases from $5x10^{17}$ cm^{-3} to $2x10^{18}$ cm^{-3}. For the same changes in [B], the photoconductivity varies by only a factor of 10. As noted above, and as shown in Fig. 2.1(a) the dark conductivity changes by about four orders of magnitude for this factor of four change in [B].

There are several factors that warrant additional discussion. The first relates to the deposition of B-compensated, near-intrinsic μc-Si. There are two factors that can play significant roles: i) the effective density of donor-like native defects; and ii) the ability to add relatively small and controlled amounts of B-atoms to the μc-Si film. LeComber et al.[6] have estimated that the density of donor-like defects in their as-

deposited, GD μc-Si films is ~2-4x10^{18} cm^{-3}. This is consistent with the observation that as-deposited dark conductivities in these films are about 2x10^{-2} S/cm. The Remote PECVD films had a lower as-deposited dark conductivity, ~6x10^{-4} S/cm, which is also consistent with the fact that a B-concentration of about 5x10^{17} cm^{-3} was required for *exact numerical compensation*. Since the conductivity ratios of these as-deposited films are greater than the ratio of the relative donor-like defect concentrations, we conclude that the relationships between the dark conductivity, and the defect-site and compensation doping densities are not simply determined by considerations of *exact numerical compensation*. We propose that the origin for these differences is in the inherently diphasic character of the μc-Si films; e.g., the interfaces. We are currently developing a model for the variation of dark conductivity through the compensation point which takes into account defects associated with i) dangling bonds in the a-Si:H material, and ii) defect states at the crystallite boundaries. The relative energies of these defects, and the ratio of the Debye length to the crystallite size will both play significant roles in determining how the addition of active B-acceptors will serve to change the dark conductivity, and the dark conductivity activation energy.

The second issue relates to the controlled incorporation of dopant atoms to compensate native donor-like defects. From the data in Fig. 2.1(b), this window is narrow. Our experience with deposition chamber histories indicates that if B-compensated intrinsic μc-Si layers are to be used in device structures, then they should be deposited in a dedicated chamber that is not used to deposit other more heavily doped p-type or n-type μc-Si layers, or Si,C alloy films. Unfortunately, we have only one chamber available for all of our amorphous Si and microcrystalline Si related studies.

The variation of the photoconductivity as a function of either the B-atom concentration, or the dark conductivity activation energy raises questions relative to the way the photoconductivity is to be interpreted. In the a-Si:H system, the photoconductivity shows a significant decrease as the dark conductivity transport mechanism changes from electron to hole dominated[7]. This decrease is approximately three orders magnitude. In contrast, and from the data in Figs. 2.1(a) and (b), the photoconductivity in the μc-Si does not show a similar drop as the material changes from electron-dominated dark conduction to hole-dominated dark conduction, i.e., from n-type to p-type. The magnitude of the dark conductivity, when normalized to

the incident photon flux, and in particular to fraction of that radiation that is capable of producing hole-electron pairs, suggests that the photoconductive gain is high, and consistent with either electron-dominated transport, or equivalently with two carrier transport over the range of compositions studied. This is also consistent with the results of experiments on p-i-n structures that have been fabricated using the B-compensated μc-Si as the i-region material[2,3]. These experiments have yielded relatively high short circuit current densities, ~5-10 mA/cm^2 to 0.5 AM1 radiation, indicating a significant two carrier current flow in the i-region material.

We have observed that the intrinsic μc-Si exhibits a high photoconductivity, but no *detectable* Staebler-Wronski effect. There are two possible explanations: i) the defect density in the B-compensated μc-Si is too high, in the sense that it masks any ability to detect light-induced defects; or ii) the recombination process that terminates the life-time of a photo-generated electron-hole pair does not occur in the amorphous regions between the crystallites. The relatively high photoconductivity, and the fact that it is dominated by electrons over a doping range that includes a transition from n-type to p-type, suggests that recombination may be dominated by centers at the interface between the crystalline and amorphous components of the μc-Si, or within the crystallites themselves. The kinetics of an interface dominated process would be influenced by the offsets at the respective band edges, as well as any band-bending that favors trapping of the holes. A similar argument could apply to hole-trapping within the crystallites; however, this is not likely due to the performance of the B-compensated material in p-i-n solar cells.

REFERENCES

1. C. Wang, M.J. Williams and G. Lucovsky, J.Vac. Sci. Technol. **A9** (1991) 444.

2. G. Lucovsky, C. Wang and M.J. Williams, Solar Cells **30** (1991) 419.

3. M.J. Williams, C. Wang and G. Lucovsky, at International Conference on Stability of a-Si:H, Denver, CO, Feb. 20-22, 1991.

4. G. Lucovsky and C. Wang, MRS Symp. Proc. **219** (1991) in press.

5. M.J. Williams, C. Wang and G. Lucovsky, MRS Symp. Proc. **219** (1991) in press.

6. P.G. LeComber, G. Willeke and W.E. Spear, J. Non-Cryst. Solids **59&60** (1983) 795.

7. P.G. LeComber and W.E. Spear, in *Amorphous Semiconductors*, ed. by M.H. Brodsky (Springer Verlag, Berlin, 1979), p. 251.

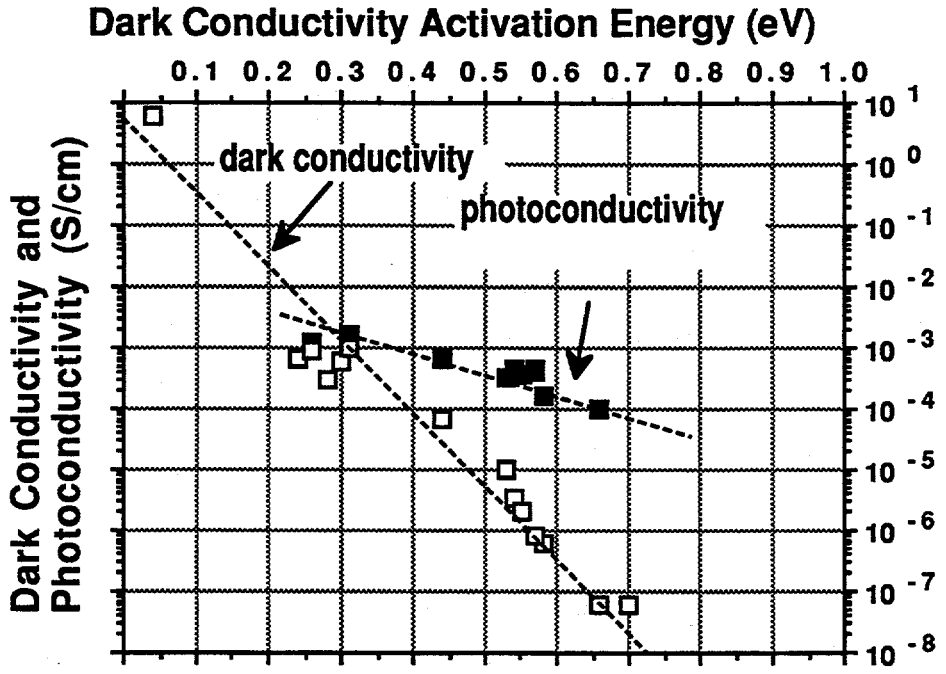

Fig. 2.1(a) Dark and Photoconductivity vs activation energy for boron-doped mc-Si

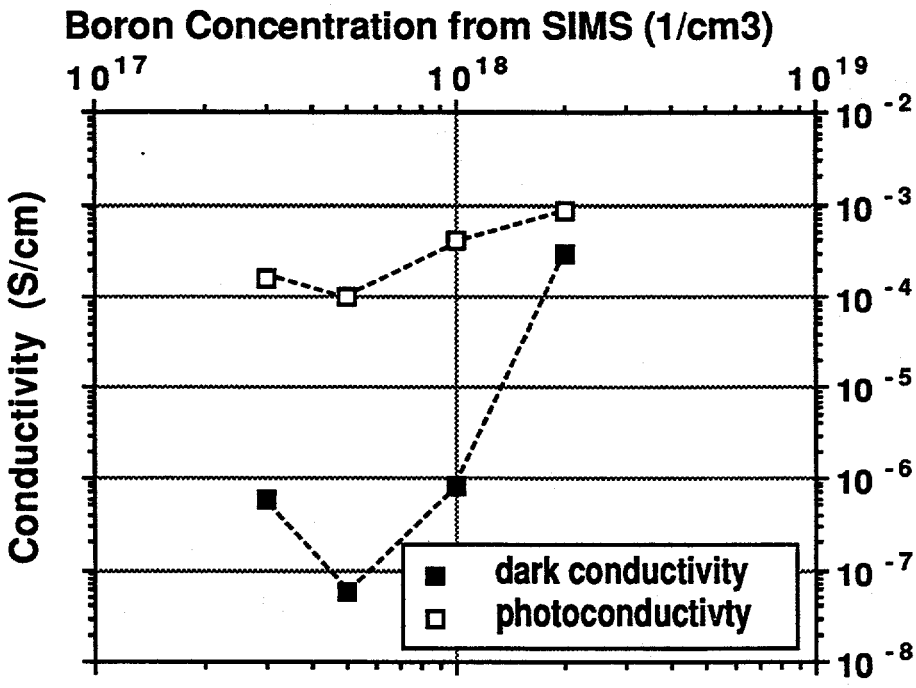

Fig. 2.1(b) Dark conductivity and photo-conductivity versus boron concentration

3. Deposition of a-Si,C:H and μc-Si,C alloys by Remote PECVD

We have extended the remote PECVD process to the deposition of undoped and doped a-Si,C:H and μc-Si,C alloy films. This has been accomplished by adding the carbon atom source gas, CH_4, downstream, along with the Si and dopant atoms sources, and for the case of μc-Si,C, also downstream injection of H_2. We have compared the dark conductivities of the a-Si,C:H and μc-Si,C alloy films, respectively, with those of a-Si:H and μc-Si, and have been shown that the decreased conductivity of the Si,C alloy films can be attributed to the wider band-gaps of the Si,C alloys. For the case of the μc-Si,C films this means that the dark conductivities are also limited by thermal emission of carriers from the Si crystallites into the a-Si,C:H material that separates the Si crystallites.

The conditions for depositing a-Si,C:H films are essentially the same as those used for device-quality a-Si:H films, except that the C-atom source gas CH_4 is introduced downstream along with the Si-atom source gas SiH_4, and the combined flow of the SiH_4+CH_4 mixture is maintained at a level comparable to the flow of SiH_4 for the a-Si:H depositions. We define the SiH_4 fraction of these gas mixtures as X = SiH_4/(SiH_4+CH_4), and have varied X between 1.0 and 0.33, to deposit a-Si,C:H films that contain up to ~15 at.% C. For the deposition of the μc-Si,C:H alloy films, a flow of 30 sccm of molecular hydrogen, H_2, was added downstream to the SiH_4/CH_4 source gas mixture. For the deposition of doped a-Si,C:H or μc-Si,C:H, the dopant-atom source gases, diborane, B_2H_6, and phosphine, PH_3, were premixed with the Si- and C-atom source gases and also injected down-stream.

A series of a-Si,C::H alloy films with different C-atom concentrations has been deposited by varying X between 1 and 0.33. The local bonding in these films was characterized by IR absorption. The spectral features specifically associated with C-atom incorporation have been discussed elsewhere[1]. These IR features include bond-stretching and bending absorptions due to Si-C, CH_3 and C-SiH groups. Each of these spectral features increases in strength as the CH_4 fraction in the source gas mixture is increased, i.e., as X decreases from 1.0 to 0.33.

We have also studied the electrical and optical properties of this same series of a-Si,C:H alloy films[1-3]. The dark conductivity, the photo-conductivity and the effective optical bandgap are essentially the same as those in a-Si,C:H alloy films deposited by

the GD method using comparable SiH_4/CH_4 source gas mixtures. The bandgap and photoconductivity data indicate that as X decreases from 1 (a-Si:H) to 0.5, the E_{04} bandgap increases from ~1.90 eV to ~2.25 eV, and the photoconductivity for illumination by white light at ~50 mW/cm^2, decreases from $5.5x10^{-5}$ S/cm to $8.9x10^{-9}$ S/cm, both effects similar to the results reported for GD films. E_{04} is 2.05 eV for the undoped X = 0.67 a-Si,C:H.

As stated above, p-type and n-type a-Si,C:H alloy films have been deposited by adding the dopant atom gases to the downstream injected SiH_4/CH_4 gas mixture. The most extensive of these studies have been confined to a single SiH_4/CH_4 source gas mixture, X = 0.67. For the highest diborane doping gas ratio used, (1%), and for X = 0.67, the conductivity of the p-type a-Si,C:H was $1.4x10^{-6}$ S/cm with an activation energy of 0.46 eV. This conductivity is about a factor of 500 less than what is obtained in a-Si:H for the same doping gas fraction. The decreased dark conductivity is consistent with an increased activation energy: 0.46 eV in a-Si,C:H, and 0.31 eV in a-Si:H. For the highest phosphine doping gas ratio, also (1%), the dark conductivity was $3.5x10^{-5}$ S/cm with activation energy of 0.41 eV. This is about a factor of 570 less than that of a-Si:H grown from the same relative concentration of PH_3. The decreased conductivity is also in accord with an increased activation energy: 0.41 eV as compared to 0.25 eV. This means that the smaller conductivities for the doped a-Si,C:H as compared to a-Si:H result mostly from the larger activation energies[2,3], and the conductivity prefactors, which characterize transport in extended states of the conduction and valence bands of a-Si,C:H, are essentially the same as in a-Si:H.

μc-Si,C:H alloy films have been deposited by RPECVD by adding H_2 to the downstream injected SiH_4/CH_4 source gas mixtures. The combined effective flow rate of the SiH_4/CH_4 mixture was maintained 1~2 sccm, and the flow rate of the H_2 was fixed 30 sccm, the same ratio as used for the deposition of the μc-Si films with the highest fraction of crystallinity. The degree of crystallinity in the μc-Si,C:H alloy films has been investigated by Raman spectroscopy (Fig. 3.1) and transmission electron microscopy (TEM) (Fig. 3.2). Studies by TEM imaging and Raman scattering indicate a decreased amount of crystallinity in μc-Si,C:H as compared to μc-Si prepared under similar deposition conditions. Raman spectra for μc-Si,C:H, and for a-Si,C:H alloy films deposited on fused silica are displayed in Fig. 3.1, and show that μc-Si,C:H alloy films exhibit a sharp feature at 520 cm^{-1} that is the same as the sharp crystalline feature

found in μc-Si films. This establishes that at least one of the possible crystalline components in these films is Si. The fraction of crystallinity can be estimated from the ratio of the Raman scattering in the crystalline "TO" feature to that in the 470 cm^{-1} "TO" band; for the film shown in Fig. 3.1 this is ~10-20%. We have obtained the Raman spectrum over a spectral range from about 100 to 1500 cm^{-1}, and have found no evidence for spectral features associated with crystalline SiC, or with either of the crystalline forms of carbon: diamond or graphite. This means that the C-atoms incorporated into the μc-Si,C:H alloys must then be included in the amorphous material that is interposed between the Si crystallites. This interpretation of the Raman and TEM data is supported by the IR spectra discussed in Ref. 1. Furthermore, by adding additional CH_4 into the source gas mixtures that include H_2, the degree of crystallinity of deposited alloy films decreases. Hydrogenated amorphous carbon films have been deposited under the same deposition conditions but with no SiH_4 in the source gas mixture, and with the flow rate of H_2 maintained at 30 sccm.

TABLE 3.1 Properties of Si,C Alloy Films

X	Doping Gas Ratio	Dark Cond. (S/cm)	E_a (eV)
0.67	PH_3, 0.1%	5.6e-2	0.10
0.50	PH_3, 0.1%	1.0e-3	0.22
0.33*	PH_3, 0.1%	6.2e-13	0.91
0.67*	PH_3, 1.0%	1.3e-3	0.23
0.67	B_2H_6, 0.1%	6.3e-4	0.18
0.50	B_2H_6, 0.1%	1.1e-6	0.44
0.33*	B_2H_6, 0.1%	8.2e-10	0.73
0.67*	B_2H_6, 1.0%	1.4e-7	0.56

* these films are amorphous even though they were deposited using H_2

adding additional CH_4 into the source gas mixtures that include H_2, the degree of crystallinity of deposited alloy films decreases. Hydrogenated amorphous carbon films have been deposited under the same deposition conditions, but with no SiH_4 in the source gas mixture, and with the flow rate of H_2 maintained at 30 sccm.

Deposition of heavily doped, p-type and n-type μc-Si,C:H alloy films also has been accom-plished by RPECVD, however for a limited set of gas flow conditions. The

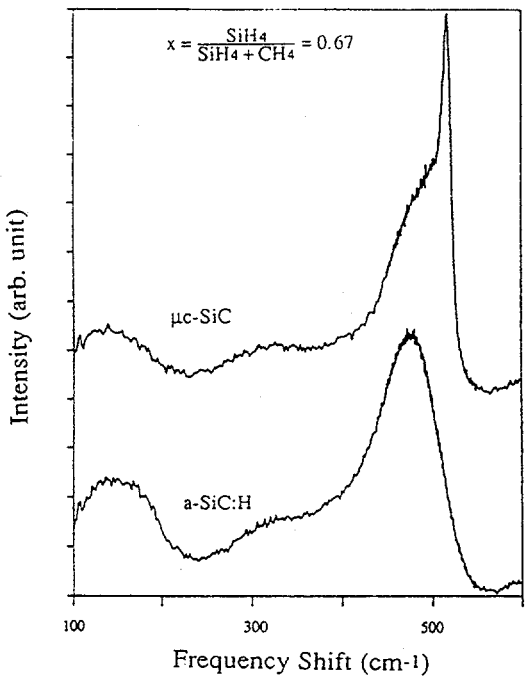

Figure 3.1
Raman Spectra of a-Si,C:H and μc-Si,C

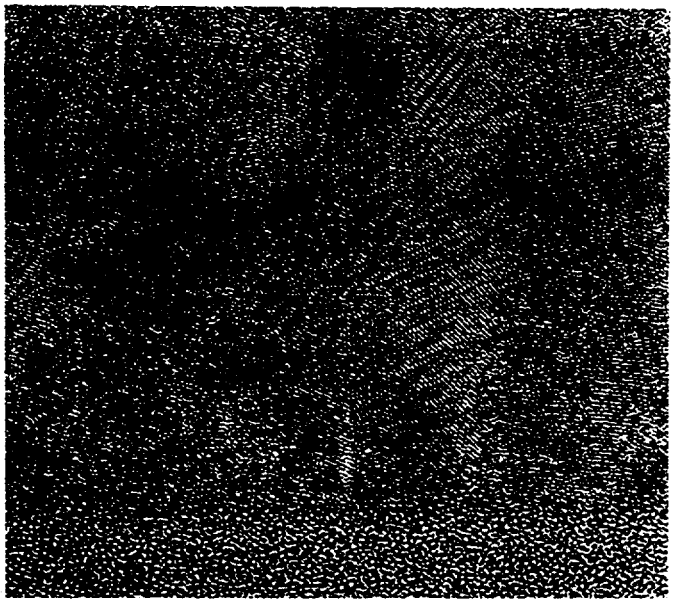

Figure 3.2
TEM Micrograph of μc-Si/SIO_2 interface.
SiO_2 on bottom; μc-Si on Top

dopant atom source gas, either diborane or phosphine, was added to the Si- and C-atom source gas mixture at concentrations of 0.1% and 1%, and for X = 0.33, 0.5 and 0.67. Table 3.1 summarizes the results of these depositions. Films deposited with 1% *gas phase doping* of the X = 0.67 Si-atom and C-atom source gas mixture were amorphous as determined by analysis of the Raman scattering. Films deposited from 0.1% doping gas mixtures were microcrystalline for X = 0.67 and 0.50, but became amorphous when the silane fraction was further reduced to 0.33. Raman scattering was also the characterization technique used to distinguish between the amorphous and microcrystalline character of these less heavily doped films. We have also studied the properties of undoped Si,C alloy films grown under flow conditions which included 30 sccm of H_2. μc-Si,C:H films were obtained for X = 0.67 and 0.50, but not for X = 0.33. It is interesting, and important to note that the doped and undoped a-Si,C:H alloys that are produced with H_2 dilution of the SiH_4/CH_4 mixtures have properties which are generally different from a-Si,C:H films produced without the H_2 flow. For example, the conductivity of p-type a-Si,C:H films deposited with a gas phase doping fraction of 1.0% differ by a factor of 10, with the film grown without H_2 dilution having the higher conductivity and lower activation energy. This is consistent with the fact that hydrogen atoms can, under certain circumstances combine with dopant atoms to produce local bonding configurations that reduce the doping efficiency of the B- and P-atoms. However, as noted above (in Section 2), the dark conductivities of p-type a-Si:H films, deposited with, and without H_2 dilution were essentially the same.

REFERENCES

1. G. Lucovsky, C. Wang and M.J. Williams, Solar Cells **30** (1991) 419.

2. G. Lucovsky and C. Wang. MRS Symp. Proc. **219** (1991), in press.

3. C. Wang, G. Lucovsky and R.J. Nemanich, MRS Symp. Proc. **219** (1991), in press.

4. Transport Mechanisms in Si and Si,C Amorphous and Microcrystalline Films

We have analyzed the dark conductivity transport data for undoped and doped a-Si:H, a-Si,C:H, μc-Si and μc-Si,C films and have concluded that the transport in the microcrystalline films is limited by either one of two mechanisms: i) thermionic emission over energy barriers at the boundaries of the crystalline and amorphous regions; or ii) by thermal assisted tunnelling from the crystallites into band tail states of the amorphous components. Analysis of data in terms of these two mechanisms

explains the relatively high dark conductivities that can be obtained in μc-Si, ~5-100 S/cm and identifies a significant limitation on the attainment of conductivities higher than 0.1 S/cm in Si,C alloy films with bandgaps greater than about 2.0 eV.

Table 4.1: Electrical Properties of Films grown by Remote PECVD

Material	H_2/SiH_4 ratio	Dopant Gas/ SiH_4 ratio	Dark Conductivity (S/cm) = $(\Omega cm)^{-1}$	Activation Energy (eV)
a-Si:H	0	0	2.4×10^{-10}	0.80
a-Si:H(n)	0	1×10^{-2}	2.0×10^{-3}	0.25
a-Si:H(p)	0	1×10^{-3}	4.0×10^{-7}	0.59
a-Si:H(p)	0	1×10^{-1}	2.4×10^{-3}	0.31
μc-Si	30:1	0	6.0×10^{-4}	0.30
μc-Si(n)	30:1	3×10^{-5}	0.2	0.08
μc-Si(n)	30:1	3×10^{-4}	5.0	0.05
μc-Si(n)	30:1	1×10^{-2}	40	0.02
μc-Si(p)	30:1	1×10^{-5}	6.0×10^{-8}	0.66
μc-Si(p)	30:1	2×10^{-4}	7.0×10^{-4}	0.24
μc-Si(p)	30:1	1×10^{-3}	6.0	0.04
a-Si:H(p)	30:1	1×10^{-2}	4.0×10^{-5}	0.40
a-Si:H(p)	30:1	1×10^{-1}	3.0×10^{-3}	0.30
a-Si,C:H	0	0	2.3×10^{-13}	0.99
a-Si,C:H(n)	0	1×10^{-2}	3.5×10^{-5}	0.41
a-Si,C:H(p)	0	1×10^{-3}	2.0×10^{-9}	0.69
a-Si,C:H(p)	0	1×10^{-2}	1.4×10^{-6}	0.46
μc-Si,C(n)	30:1	1×10^{-2}	1.3×10^{-3}	0.23
μc-Si,C(p)	30:1	1×10^{-3}	6.3×10^{-4}	0.18
a-Si,C:H(p)	30:1	1×10^{-2}	1.4×10^{-7}	0.56

Dark conductivity data is summarized in Table 4.1. These data were obtained using surface cell structures with a film thickness of ~1000Å, and an electrode spacing of 5 mm. Measurements were made at a field of 200 $V\text{-}cm^{-1}$, where the current-

voltage, I-V, characteristic is ohmic. The conductivity data display the usual activated behavior, i.e.,

$$\sigma = \sigma_0^* \exp(-E_\sigma^*/kT). \quad (1)$$

where σ_0^* is the conductivity prefactor and E_σ^* is an effective activation energy. Figure 4.1 is a plot of σ_0^* versus E_σ^* which demonstrates the usual Meyer-Neldel behavior[1];

$$\sigma_0^* = C \exp (E_\sigma^*/E_0), \quad (2)$$

There are two things to note: i) the data for all of the a-Si,C:H with E_σ^* >0.2 eV display a linear dependence with C ≈ 3±1 S/cm and E_0 = 0.11±0.02 eV; and ii) the fit to the μc-Si films with < 0.1 eV is described by different constants, C ≈ 275 S/cm and E_0 ≈ -0.020 eV. The data in Fig. 4.1, and those presented below in Figs. 4.2 and 4.3 are for undoped, n-type and p-type films. Figure 4.2 contains a plot of σ_{rt} vs. E_a for all of the Si and Si,C alloy films listed in Table 4.1, and can be fit with two exponential functions of the form:

$$\sigma_{rt} = \sigma_0^* \exp (-E_\sigma^*/kT_{eff}). \quad (3)$$

For the Si and Si,C films with E_σ^* > 0.2 eV, σ_0^* ≈ 5 S/cm = and T_{eff} = 390K, whereas for the four μc-Si films with < 0.1 eV, σ_0^* ≈ 300 S/cm and T_{eff} ≈ 125K. He et al. have reported similar data for doped μc-Si[2]. The values of T_{eff} from Fig. 4.2, are consistent with the constants determined from the Meyer-Neldel fits, since;

$$kT_{eff} = (E_0\, kT) / (E_0 - kT), \quad (4)$$

where T = 300K. The data for a-Si:H, and for μc-Si with > 0.2 eV also follow a Meyer-Neldel behavior with essentially the same constants as the Si,C alloys.

There is another aspect of the conductivity data illustrated in Fig. 4.3 where we have plotted activation energies for a-Si,C:H and μc-Si,C, E_σ^*(Si,C), as a function of the *corresponding* activation energies for a-Si:H and μc-Si, E_σ^*(Si), for films that have been deposited using the same ratios of dopant gas to either the Si- atom, or the Si-atom plus C-atom source gas mixtures. These data display a linear relationship:

$$E_\sigma^*(Si,C) = E_\sigma^*(O) + \alpha\, E_\sigma^*(Si) \quad (5)$$

where E_σ^*(O) = 0.167 eV and α = 0.998; the fit parameter R^2 = 0.98.

Three aspects of the experimental data are used for the development of the model for the carrier transport: i) the microstructure, including the chemical nature of the crystalline and amorphous components; ii) the commonality of the Meyer-Neldel plots for all of the materials with E_σ^* > 0.2 eV; and iii) the linear relationship between E_σ^*(Si,C) and E_σ^*(Si). We start with some comments relative to transport in two phase materials.

Table 4.2: Band Offsets for μc-Si and μc-Si,C

Band offset Material	Conduction Band E_C(amorphous) - E_C(crystal) (±0.05 eV)	Valence Band E_V(amorphous)-E_V(crystal) (±0.05 eV)
a-Si:H to c-Si	+ 0.25 eV	- 0.30 eV
a-Si,C:H to c-Si	+ 0.40 eV	- 0.50 eV
Difference in Offsets	0.15 eV	0.20 eV

There has been extensive modelling of carrier transport in two phase materials; much of this has been reviewed in Ref. 3. Fig. 4.4(a) indicates a structural model appropriate for diphasic microcrystalline materials, and Fig. 4.4(b) gives an equivalent circuit derived from that microstructure[3]. We designate ρ(2) as the resistivity of the amorphous component and ρ(1) as the resistivity of the crystalline component. Using the data in Table 4.1, we assume for the same gas phase doping ratio that ρ(2) » ρ(1); i.e., that the dopant atoms are present in both phases of the material, and that the conductivity of the crystalline Si phase is significantly higher than for either the corresponding a-Si:H or a-Si,C:H phase. Following the model developed in Ref. 6, we then treat the microcrystalline materials as arrays of back-to-back Schottky barriers in which the doped crystalline components are *pseudo-metals*, or free-carriers reservoirs, and the doped amorphous regions separating them are the *more resistive* semiconductors. The barriers are actually n^+/n^- heterojunctions with the n^+ c-Si having the lower resistivity. The potential configuration for this heterojunction structure is equivalent to that of a Schottky barrier. For this limiting case, the resistivity of the diphasic microcrystalline material, ρ*, is approximated by[3]:

$$\rho^* \approx \{n(1)\, q\, \mu_b\}^{-1} \qquad (3)$$

where n(1) is the free-carrier concentration in the crystalline material, and μ_b is an effective mobility for the transport of free carriers from the crystalline material through the amorphous regions. If thermionic emission over interfacial barriers limits the current, then the effective mobility is thermally-activated and given by:

$$\mu_b = \mu_o \exp(-E_b/kT) \qquad (4)$$

where μ_o is an *effective* band mobility in the amorphous material, and E_b is an

effective barrier height at the crystalline/amorphous interface. Eb has two contributions: the band off set, and the relative position of the Fermi level in the crystalline and amorphous components. For heavily doped crystalline Si, we neglect the small energy differences between the Fermi position and the band edge. The interpretation for μ_b via Eqn. (4) is not unique, and one can associate the exponential dependence with an effective carrier concentration: i.e., $n = n(1) \exp(-E_b/kT)$ is the density of carriers that are thermally excited over the interfacial barrier[3]. If thermionic field-emission, involving direct tunnelling into band-tail states is the dominant mechanism, then these interpretations for E_b need some obvious reinterpretations.

To specify the particular carrier transport mechanism across the interface, we develop a model for the band-alignment at the conduction and valence band edges. We start with the band diagram for intrinsic μc-Si shown in Fig. 4.5(a). This was constructed as follows: i) since both constituents are Si, we assume that the respective Fermi levels in each phase are at mid-gap, and line-up with respect to each other; ii) we assume an effective gap for crystalline Si of ~1.2 eV, consistent with the 50 to 300Å crystallite size; iii) we use optical data to set the band gap of a-Si:H at ~1.8 eV; and finally iv) we use the doping studies of LeComber and Spear[4] to define the spread of band-tail states into the gap. For the μc-Si,C band alignment diagram in Fig. 4.5(b), we assume in addition: i) that Fermi level alignment is maintained in spite of the small (~10 at.%) incorporation of C in the amorphous phase; ii) an effective gap of ~2.1 eV; for a-Si,C:H; consistent with optical data for our samples; and iii) that band-tailing into the gap derives primarily from the local atomic disorder and is effectively the same in a-Si,C:H as in a-Si:H. These assumptions fix the conduction and valence band off set energies given in Table 4.2. The average of these is 0.175 eV, and is approximately equal to the energy intercept of 0.167 eV for the fit to the data in Fig. 4.3. Since the data in Fig. 4.3 include both n-type and p-type a-Si:H and a-Si,C:H, the intercept from Fig. 4.3, and the observation that $\alpha \approx 1.0$ means that to a good approximation the Fermi level positions in similarly doped a-Si:H and a-Si,C:H are displaced relative to each other by the average band off set energy. Stated differently, for a given gas phase doping, the Fermi level shift relative the middle of the gap is the same for a-Si:H and a-Si,C:H. This interpretation of the data in Fig. 4.3 is consistent with the Meyer-Neldel relationships shown in Fig. 4.2. The accepted interpretation of the Meyer-Neldel rule is that it derives from a statistical shift of the Fermi level through the distribution of states in the pseudo-gap[1]. A common rule for a-Si:H, a-Si,C:H and μc-Si ($E_\sigma^* > 0.2$ eV) and μc-Si,C means that relative to the center of the pseudo-gap the

densities of states in a-Si:H and a-Si,C:H are essentially the same. Figure 4.5(d) indicates the interfacial alignment of the conduction bands for light and degenerate doping in μc-Si,C. Using the data in Tables 4.1 and 4.2, the Fermi level in the crystalline component, never lines up within the distribution of band-tail states in the amorphous component so that direct tunneling into these states does not occur. We assume that for transport to involve these band-tail states the tunnel injection must be no more than a few kT below the extended states of the a-Si,C:H. Since these conditions for tunneling are not met in μc-Si,C, thermionic emission over the barrier limits the carrier transport. All of the measured activation energies in the Si,C materials are consistent with this picture: they are ≥ 0.18 eV, and therefore > 7 kT. The conductivity measurements were made at low fields, ~200 V-cm^{-1}, where the I-V characteristics are linear. This is consistent with a barrier limited ohmic transport process since the average potential drops across the barrier, and over the entire extent of the amorphous region are significantly smaller than the kT for small applied fields [6]. Average fields in excess of 10^4 V-cm^{-1} would be required to drive the I-V characteristics into a non-ohmic behavior.

The situation in the Si-materials is qualitatively different, with two exponential relationships being required to describe all of the data. Consider first the a-Si:H and μc-Si films with activation energies > 0.2 eV. The exponential parameters that fit these data are similar to those for the Si,C alloy films, and we interpret this to mean that thermionic emission over interfacial barriers applies to these materials as well. The fit parameters to the second exponential region in Fig. 4.2, for activation energies less than 0.1 eV are markedly different. The same holds for the Meyer-Neldel plot in Fig. 4.1. The observation T_{eff} has decreased significantly the below room temperature value, and the interpretation of this parameter in terms of a negative value of E_0 in the analysis of the Meyer-Neldel plot indicate that field-emission into the band tail states of the a-Si:H from the c-Si component has become the dominant transport process.

The agreement between the empirically determined band off set model, and the conductivity data establish a fundamental limitation for carrier transport in doped μc-Si,C alloys that will restrict the use of these films in many applications. Because the μc-Si,C alloys are composed of Si crystallites embedded in an a-Si,C:H matrix, increasing the C-concentration to increase transparency will increase the effective band off sets at the conduction and valence band edges, thereby making transport via thermal emission over these barriers dominate over field-emission through the

barriers. Combined with deeper effective impurity states for P and B in Si,C materials [8], this means that the conductivities of doped μc-Si,C with effective band gaps greater than about 2.0 eV will generally always be less than those of similarly doped a-Si:H films. We are studying a-Si,C:H and μc-Si,C films with increased band-gaps, ≈ 2.3 eV, to further test the trends predicted by the proposed band alignment model.

REFERENCES

1. W. Beyer and H. Overhof, in *Semiconductors and Semimetals, Vol. **21C***, ed by J.I. Pankove (Academic Press, New York, 1984), p. 257.
2. Y. He, Y. Yen, R. Wu and K. Chen, J. Non-Cryst. Solids **59&60**, 831 (1983).
3. J.W. Orton and M.J. Powell, Repts. Progr. Phys. **43**, 1263 (1980).
4. P.G. LeComber and W.E. Spear, AIP Conf. Proc. **31**, 284 (1976).

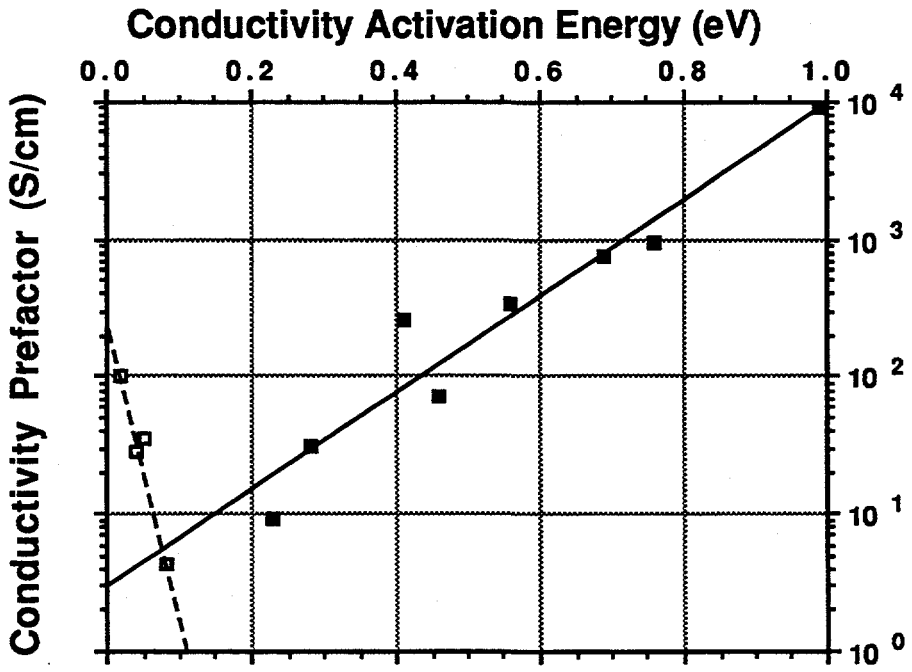

Fig. 4.1 Prefactor vs Activation Energy
Si,C (solid) and doped mc-Si (open)

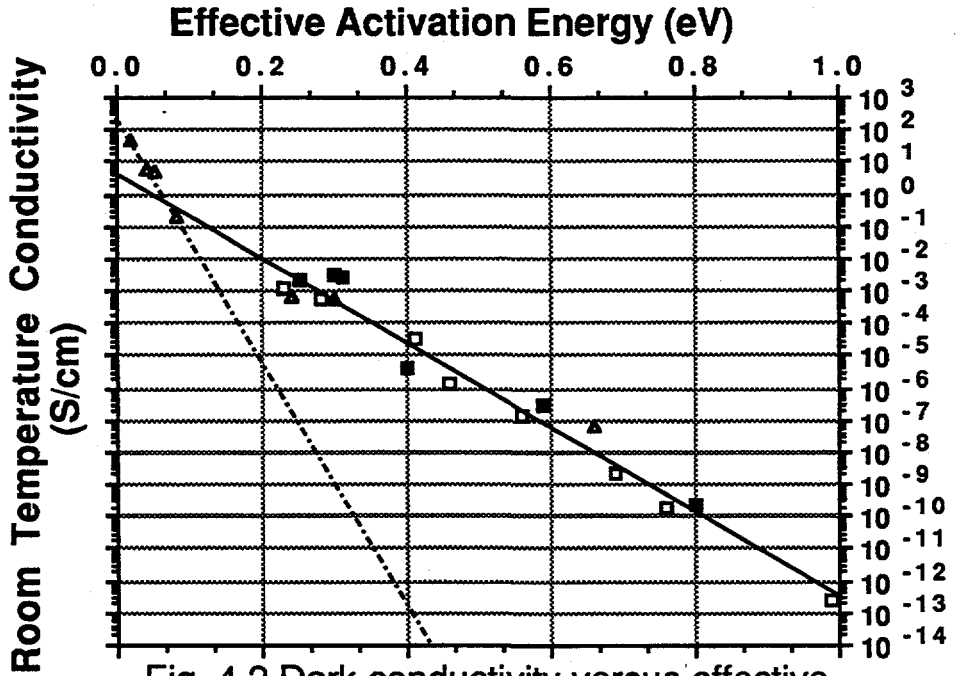

Fig. 4.2 Dark conductivity versus effective
activation energy for Si and Si,C films

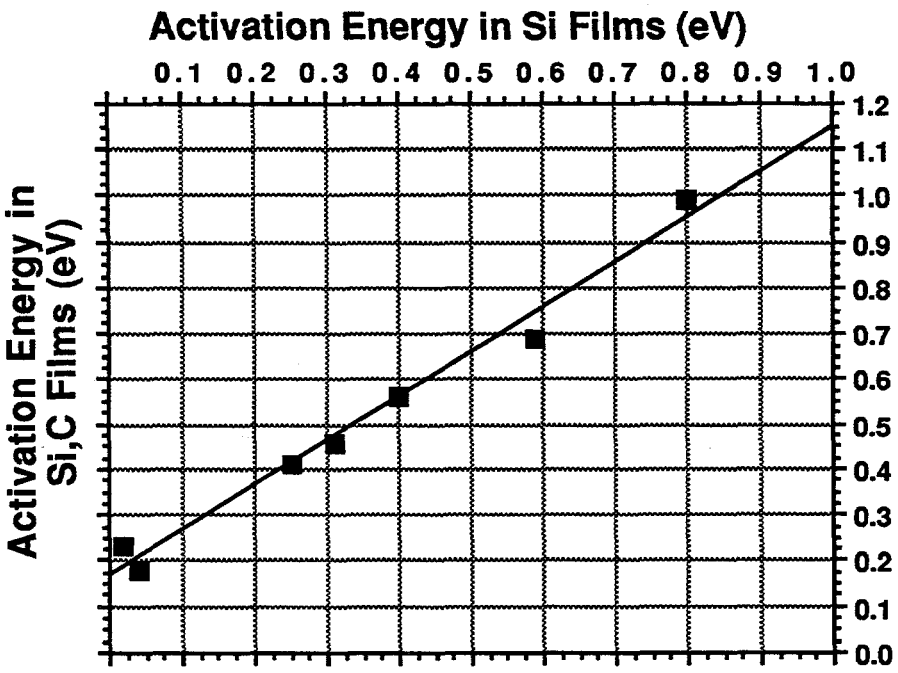

Fig. 4.3 Correlation between conductivity activation energies in Si,C and Si thin films

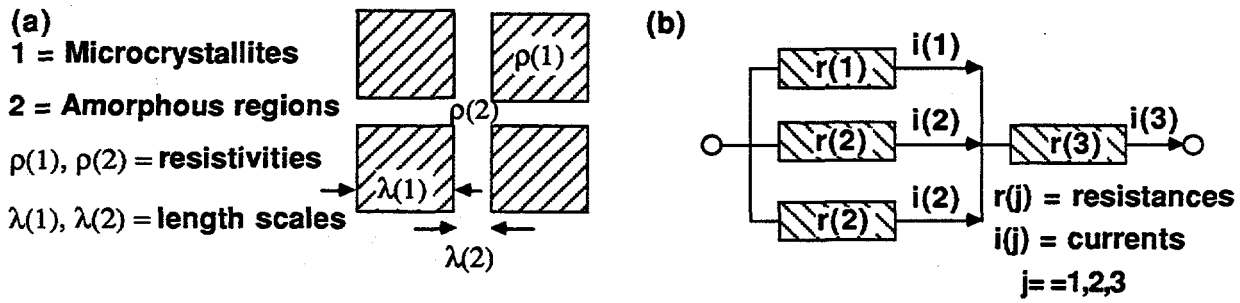

Fig. 4.4: (a) Representation of microcrystallites and amorphous regions of microcrystalline thin films. (b) Equivalent circuit for microcrystalline thin films.

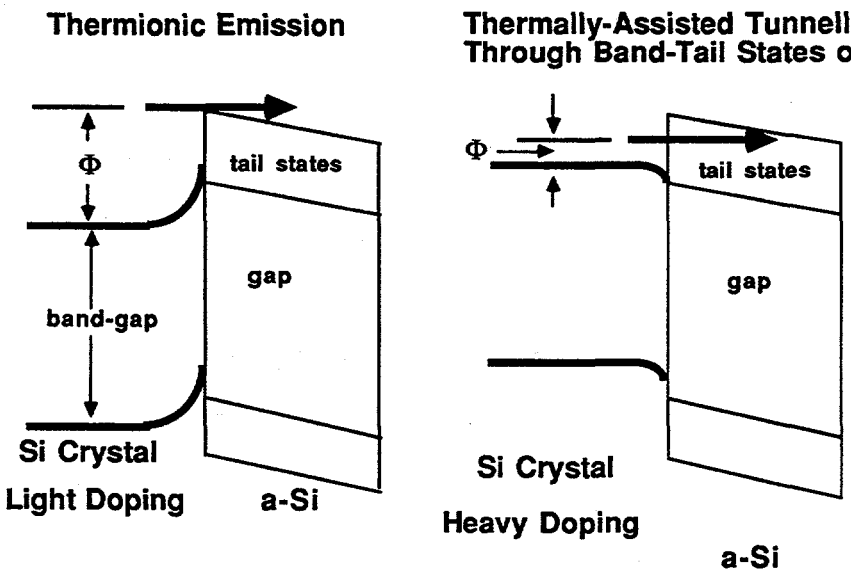

Figure 4.5: Band diagrams for the transport from the Si crystals into the a-Si:H or a-Si,C:H. For the Si system the band off-sets are comparable to the spread of the a-Si band-tail states into the gap. For the Si,C system the band off-sets are larger than the tail state spread.

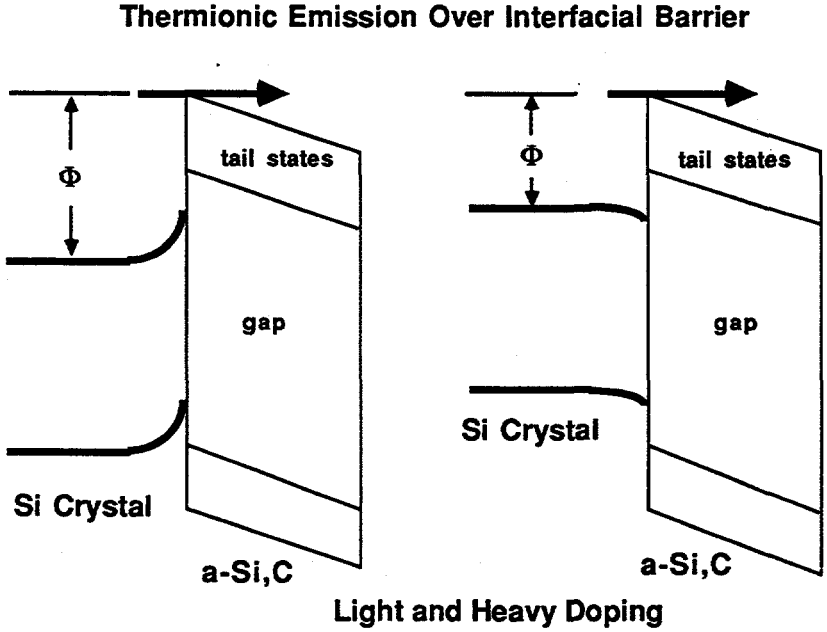

5. Formation of Device Structures using doped a-Si:H and μc-Si

We have studied the properties of doped a-Si:H and μc-Si in MOS capacitors using ~10 Ω-cm p-type crystalline substrates and thermally grown SiO_2 dielectric layers. These studies have provided information about the electron affinities of a-Si:H and μc-Si, and the effective Debye lengths in μc-Si films with different levels of p-type and n-type doping. This information is important in the design of solar cell structures that utilize the doped a-Si:H or doped μc-Si in the p- and n-layers of p-i-n structures.

We have prepared heavily-doped n-type and p-type a-Si:H and μc-Si by Remote PECVD, and have used these materials as electrodes in MOS capacitors. Shifts in the flatband voltages of MOS devices with μc-Si electrodes relative to that of a reference Al/SiO_2/c-Si device are reported and used to define effective electron affinities for the a-Si:H and μc-Si. In addition, shifts in V_{FB} are reported for capacitors with electrodes of varying dopant concentrations which can not be attributed to differences in the Fermi levels alone.

Table 1 describes the doping gas/SiH_4 ratios and the electrical properties of the μc-Si films deposited for this study[1]. Note that at dopant gas/SiH4 ratios greater than $1x10^{-3}$, p-type films are amorphous, while n-type dopant atoms can be incorporated at ratios as high as $1x10^{-2}$.

TABLE 5.1. Conductivities, σ, and activation energies, E_σ

	Dopant gas/Si H_4 ratio	σ (S/cm)	E_σ (eV)
p^+ μc-Si	$1x10^{-3}$	6.0	0.04
p μc-Si	$2x10^{-4}$	$7x10^{-4}$	0.24
n^+ μc-Si	$1x10^{-2}$	40	0.02
n μc-Si	$3x10^{-4}$	5.0	0.05

MOS capacitors were formed on p-type single-crystal Si wafers with doping concentrations of approximately $1x10^{15}$ (resistivity of 10-30 Ω-cm). Thermal oxidation of the Si substrates was performed at 950°C resulting in an oxide thickness of 250Å. The Remote PECVD process was used to deposit 700-800Å of doped μc-Si at doping

concentrations described in Table 5.1. Al electrodes were evaporated onto the μc-Si and the capacitor areas were *defined* by a wet chemical etch (HNO_3/Acetic/HF mixture) of the μc-Si using the Al dots as a mask. Finally, an Al contact was evaporated onto the backside of the sample followed by a post-metallization anneal for 30 min. at 400°C in a N_2/H_2 ambient.

The MOS devices were tested using the combined high-frequency and quasi-static C-V method. Shifts in the flatband voltages of capacitors with μc-Si electrodes with respect to an Al/SiO_2/c-Si reference were observed. Analysis of the C-V data indicates that neither the density of interface trapped charge nor the mobile charge in the oxide were changed by the deposition of doped μc-Si. These properties must therefore be determined by the oxidation process and are not influenced by any shifts in the flatband voltages.

The addition of a highly-doped μc-Si film to a stacked-gate MOS capacitor results in a shift in the flatband voltage relative to that of a Al/SiO_2/c-Si reference structure[2]. Comparing capacitors with electrodes of the heaviest doped μc-Si, p+ and n+ in Table 5.1, the relative shift in V_{FB} corresponds to an effective band gap of ~0.8 eV for the μc-Si. This is an *effective* band gap of the Si microcrystallites because of the band tail states at the conduction and valence band edges of the a-Si component of the μc-Si. The previously measured[2] effective band gap for μc-Si is 0.8 eV. Similar studies for highly doped a-Si:H electrodes give an effective band gap of 1.3 eV for the a-Si:H.

MOS capacitors have also been fabricated using lightly doped μc-Si, p and n in Table 5.1, as the gate electrode. Again, shifts are observed in the flatband voltage relative to that of the reference MOS device. However, based upon the effective activation energies of the μc-Si for the various doping levels, and the effective band gap of the μc-Si, these shifts can not be explained by changes in the Fermi level alone.

Figure 5.1 is the band diagram for an MOS capacitor with an n+ μc-Si electrode and a p-type c-Si substrate in the flatband condition. It is expected and assumed that the center of the μc-Si band gap aligns itself with the center of the c-Si band gap. In the case shown, the Fermi level in the n+ μc-Si is located 0.02 eV below the conduction band (based on $E\sigma$ given in Table 5.1). Assuming an effective band gap of

0.8 eV in the μc-Si, this corresponds to a distance 0.38eV from the center of the gap. The difference between the Fermi level and the intrinsic Fermi level (midgap) in the c-Si is given by[3]

$$\psi_b = \frac{kT}{q} \ln \frac{N_a}{n_i} \tag{1}$$

At room temperature and with a substrate doping of $N_a = 10^{15}$ cm^{-3}, Equation (1) yields ψ_b = -0.29 V. The ideal flatband voltage would then be the difference, or just 0.38 - (-0.29) = 0.67 V. The same derivation for a capacitor with a n μc-Si electrode and the same substrate yields an expected V_{FB} of 0.64 V. The shift in V_{FB} that is achieved by varying the doping from n to n^+ is

$$\Delta V_{FB,n} = V_{FB}(n^{++}) - V_{FB}(n^{+}) \tag{2}$$

For the case when the center of the band gap in the electrode lines up with the center of the band gap in the substrate, Equation (2) becomes

$$\Delta V_{FB,n} = E_{\sigma}(n^{++}) - E_{\sigma}(n^{+}) \tag{3}$$

By this analysis, $\Delta V_{FB,n}$ = -0.03 eV. Similarly, the shift in flatband voltage achieved by varying the electrode doping from p to p^+ is given by

$$\Delta V_{FB,p} = V_{FB}(p^{++}) - V_{FB}(p^{+}) \tag{4}$$

and is calculated from the effective activation energies to be $\Delta V_{FB,p}$ = 0.20 eV.

The measured shifts in V_{FB} deviate in magnitude from these ideal values. However, the directions of the shifts are as predicted. From high-frequency C-V measurements, $\Delta V_{FB,n}$ = -0.36 V and $\Delta V_{FB,p}$ = 1.02 V. This indicates that the observed flatband voltages can not be fully explained by the difference in the Fermi levels alone. There are two possible explanations for this: 1) positive charge in the SiO_2 and 2) the Al top electrode is influencing the flatband voltage. C-V measurements made on reference samples that were processed at the same time as those with μc-Si gates indicate that oxide charge is not a factor unless charge is introduced during the deposition of μc-Si which is unlikely. Previous studies have

shown that the influence of the Al is greater for capacitors which use highly-doped a-Si electrodes than for those with highly doped μc-Si electrodes.[1] In addition, the shifts described above for varying doping levels indicate that the Al top electrode is more likely to influence V_{FB} in capacitors with p and n (lighter doped) μc-Si electrodes, suggesting that this effect is related to the magnitude of the conductivity of the μc-Si. Because of the diphasic nature of the μc-Si, however, properties such as the Debye length are difficult to define and further investigation is required to fully understand all of the effects that must be taken into account these less-heavily doped films.

Clearly, from the data in Table 5.1 and the results reported above for V_{FB}, the p-type μc-Si films, due to the difficulty of obtaining high doping levels and therefore higher conductivities, do not perform as well as the n-type films as gate electrodes. The heaviest doped p^+ and n^+ films, on the other hand, continue to hold promise as low-temperature, alternative gate electrode materials.

Figure 5.1 also shows the band diagram for a MOS capacitor with a p-type μc-Si electrode and an n-type c-Si substrate in the flatband condition. From the assumption that the bands in the electrode and the substrate line up at their respective midgap levels, and from the measured effective band gap of the μc-Si, an effective electron affinity for the μc-Si can be determined. If the band gap of c-Si is taken to be 1.12 eV, the conduction band of the μc-Si is positioned 0.16eV below the conduction band of the c-Si. The electron affinity of the μc-Si is then the difference between the electron affinity of c-Si (4.15 eV) and this conduction band offset. This results in an effective electron affinity of 4.31eV for the μc-Si. A similar analysis of the data with a-Si:H electrodes results in an effective electron affinity of 4.06eV.

Capacitance-voltage characteristics of MOS capacitors with in situ doped Remote PECVD μc-Si and a-Si:H electrodes have been studied. Shifts in the flatband voltages between heavily doped p-type and n-type electrodes have been measured and used to derive effective band gaps and electron affinities for both the μc-Si and a-Si:H. In addition, shifts in V_{FB} obtained by varying the dopant levels in the electrodes were discussed and explained in terms of the conductive properties of the films.

REFERENCES

1. D.R. Lee, C.H. Bjorkman, et al., MRS Symp. Proc. **219** (1991) in print.

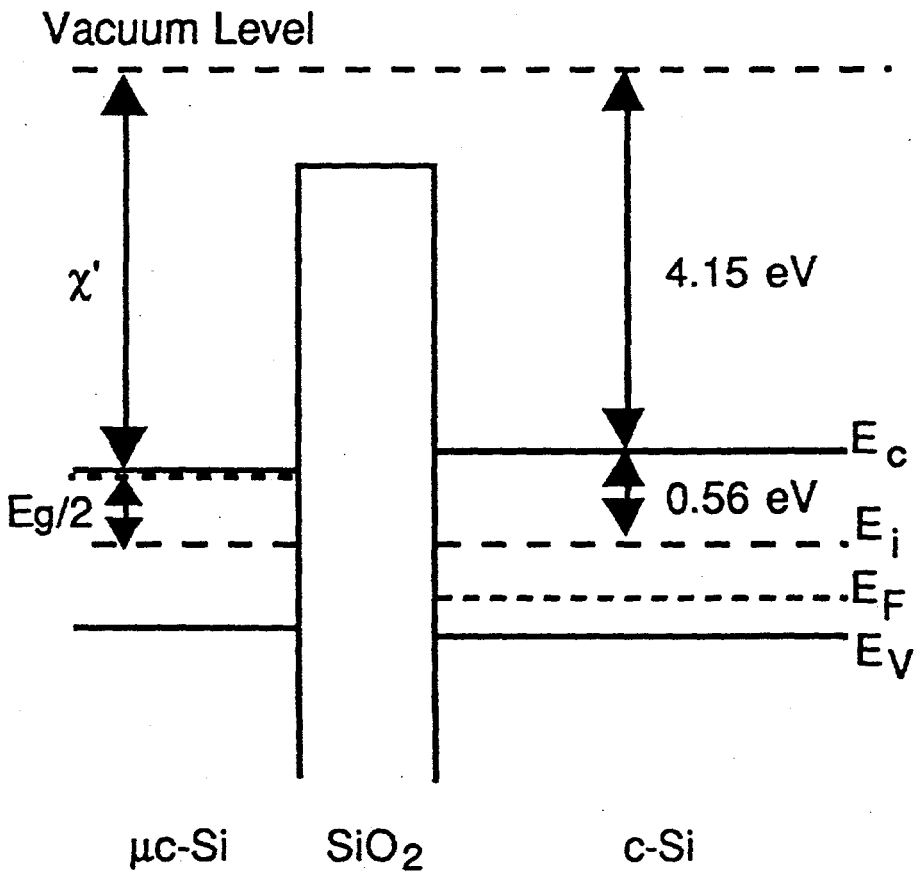

FIGURE 1

Energy band diagram for a MOS capacitor in the flatband condition.

6.1. Defect States in a-Si:H by Sub-Pico-Second Spectroscopies

We have collaborated with Professor Kurz's group a RWTH in Aachen, Germany, and have studied the contributions of process induced defect states to recombination of photogenerated electron-pairs. We find that the process induced defect states that contribute to the sub-bandgap absorption, as determined by CPM, also serve as recombination centers for an Auger type recombination process for electron-hole pairs that dominates in the sub-picosecond time regime.

We have investigated the influence of deep defect states on the picosecond decay of photoinduced absorption in a-Si:H using femtosecond laser-pulses. For device-quality a-Si:H with a low density of deep defect states, $N_d \approx 10^{16}$ cm^{-3}, the recovery of photoinduced absorption is controlled by an intrinsic bimolecular recombination process. For a-Si:H, with the same hydrogen concentration, but deposited at 40°C, and with a higher density of defect states, $N_d \approx 10^{18}$ cm^{-3}, the recovery is significantly faster and controlled by a recombination process that involves deep defect states.

The recovery of photoinduced free carrier absorption in a-Si:H on ultrashort time-scales can be controlled by non-radiative recombination through either bandtail or defect states, by shallow trapping into bandtail states, or by deep trapping into defect states associated dangling bonds[1]. While the effect of bandtail trapping on the optical response of free carriers is poorly understood, it is well known that the optical absorption cross section for electrons can be significantly reduced by trapping into dangling bond states[2]. To separate the effects of shallow trapping into bandtail states, and deep trapping into dangling bond states, a-Si:H films with different defect state densities, but with the same density and character of the bandtail states, were prepared by reactive magnetron sputtering, RMS, at different substrate temperatures but with the same partial pressure of hydrogen[3]. a-Si:H samples of 0.5 μm thickness, with bonded hydrogen concentrations, [H], of ~12-14 at.%, were deposited on fused silica substrates at 40°C, and at 250°C. The defect densities, N_d, in the as-deposited films were determined from the sub-bandgap absorbance, measured by the constant photocurrent method, CPM. N_d was about 10^{18} cm^{-3} for the film deposited at 40°C, and ~10^{16} cm^{-3} for the film deposited at 250°C. The defect density in the film deposited at 40°C could be reduced by a two hour anneal at 200°C in a dry nitrogen ambient to a level ~10^{16}cm^{-3}, essentially the same as that of film deposited at 250°C.

Other measurements have demonstrated that the optical and photoelectronic properties of these annealed films are the same as those of electronic-grade a-Si:H deposited by both the RMS and conventional glow discharge, GD, processes at temperatures in the range between 200 and 300°C [3]. In particular, the spectral dependence of the absorption for photon energies greater than approximately 1.5 eV is effectively the same for the as-deposited and annealed RMS films, as for GD and RMS films deposited at ~250°C, indicating essentially same densities and energy distributions of bandtail states. The only differences between the low temperature as-deposited and unannealed films, and the others are then in the densities of the deep defect states and the associated sub-bandgap absorption below about 1.5 eV.

Time-resolved transmission and reflectivity measurements were performed simultaneously in a standard pump-probe geometry using 50 fs-pulses at 2 eV for photoexcitation and 100 fs-pulses at 1.48 eV for probing the optical response of the photogenerated carriers[1], and references therein]. The transient change of absorption was obtained from the transmission and reflectivity data using standard thin film optical relationships[3]. Laser pulses at 2 eV were derived from a colliding pulse mode-locked dye laser[4] and were further amplified in a multipass dye amplifier, pumped by a copper-vapor laser at 7 KHz. A part of the amplified pulse train was focussed into an ethylene glycol cell to generate broadband continuum pulses. Probe pulses at 1.48 eV were isolated from the continuum source using an interference filter.

The transient change of absorption, $\Delta\alpha$, obtained from an a-Si:H film deposited at 40°C and annealed at 200°C, and with $N_d \approx 10^{16}$ cm^{-3} is displayed in Fig. 6.1. The response of this annealed film is the same as for an RMS film with the same [H] and N_d, but deposited at ~250°C. Since the photon energy of the probe pulses (E_{pr} = 1.48 eV) is below the optical bandgap in a-Si:H, the measured change in absorption is entirely due to the optical response of the photoexcited free carriers. Contributions to $\Delta\alpha$ due to changes of the lattice temperature can be neglected[1]. During the excitation pulse, $\Delta\alpha$ rises and reaches a maximum of $\Delta\alpha_{max}$ at the end of the excitation pulse. It has been previously shown[1] that $\Delta\alpha_{max}$ is linearly proportional to the density of photoexcited free e-h pairs, N_{ex}:

$$\Delta\alpha_{max} = a_c \times N_{ex} \qquad (1)$$

where a_c is the absorption cross section for e-h pairs at the probe photon energy: for E_{pr} = 1.48 eV, $a_c = 6.6*10^{-17}$ cm^2. After the end of the excitation pulse, $\Delta\alpha$ starts to

recover on a picosecond, psec, time scale. This recovery can be due to either a trapping, or a recombination process. If we assume a_c to be constant on the time scale displayed in Fig. 1, then the time evolution of $\Delta\alpha$ in Fig. 1 is consistent with the bimolecular recombination process previously reported for case of higher excitation densities[1]:

$$dN/dt = -\gamma x\, N^2 \qquad (2)$$

For this mechanism, the decrease in $\Delta\alpha$ results from a disappearance of photo-generated free carriers, rather than from any change in a_c. A model calculation based on Eqn. 2, and indicated by the solid line in Fig. 1, provides a satisfactory fit to the experimental data, with a constant of proportionality, $\gamma = 6*10^{-9}$ s/cm^3, very close to the value of $\gamma = 7*10^{-9}$ s/cm^3, obtained in our previous studies[1]. This demonstrates that for the low defect density a-Si:H, the psec recovery of photoinduced absorption is dominated by an intrinsic bimolecular recombination process. For this material, any changes of a_c due bandtail state trapping or deep defect state trapping can then be neglected.

The transient changes in absorption obtained for the a-Si:H film deposited at 40°C before and after annealing are shown in Fig. 6.2. The sub-bandgap absorption indicates a defect density in the as-deposited (unannealed) state of $N_d \approx 10^{18}$ cm^{-3}, and defect density of $N_d \approx 10^{16}$ cm^{-3} after annealing at 200°C. In the unannealed state, there is a substantial increase of the recovery rate on both psec and sub-psec time scales. Since the density of photogenerated electron-hole pairs is essentially the same as in the annealed sample discussed above, the bimolecular mechanism cannot apply since this would require a significant increase in γ, which is neither consistent with our previous studies[1], nor with the results reported above for the annealed sample (see Fig. 6.1). The increase in the recovery rate in the low temperature, as-deposited film must then be explained by a different ultrafast relaxation process: by either an e-h pair capture, or recombination process in which the increased density of deep defect states plays a significant role.

There are two types of mechanisms by which deep defect states can increase the recovery rate in the unannealed a-Si:H: (i) a capture process in which electrons (and/or holes) are trapped into the deep defect states; or (ii) an Auger-type recombination process where the recombination energy of e-h pairs is transferred to the defect state[6]. A model for the capture process, (i), predicts an induced

transparency: $\Delta\alpha$ should become negative due to trapping of electrons into D^0 states and thereby converting them to D^- states[2]. This type of induced transparency has been reported for doped a-Si:H, and is associated with trapping into deep defect states[5].

On the other hand, our experimental data are better explained by an ultrafast non-radiative recombination process, similar to the bimolecular Auger-process reported previously[1]. For example, a possible mechanism could be the recombination of an e-h pair, and the transfer of the recombination energy to a D^0 state[6]. This transfer of energy can ionize the D^0 state, producing a D^+ state, and releasing an electron into the conduction band. The net absorption change caused by this process is given by, $a_+ - a_0$, the difference between the respective optical absorption cross sections of D^+ and D^0 states[2], a_+ and a_0. Since this difference is approximately equal to, but opposite in sign to, the optical cross section of free electrons, $a_+ - a_0 \approx -a_{ce}$,[1] this type of recombination process leads to a reduction of the induced absorption even though the number of free electrons has not changed. The temporal change of absorption can thus be described by:

$$\Delta\alpha(t) = a_{ce} \times N_e(t) - (a_0 - a_+) \times N_+(t) \qquad (3)$$

where N_+ is the density of D^+ states. After the ultrafast ionization process, D^+ states can be neutralized by the capture of free electrons. Since the capture cross section for this process is very high[7], it can occur on a psec time scale. The bimolecular recombination, and the subsequent trapping processes are described by the following rate equations:

$$dN/dt = -\xi^*(N_d - N_+) \times N_e - \gamma \times N^2 \qquad (4)$$

$$dN_+/dt = \xi^*(N_d - N_+) \times N - \sigma \times N_+ \times N_e \qquad (5)$$

where ξ is the recombination coefficient for the defect-related recombination process, and σ is the capture rate for electrons into the D^+ states.

In Fig. 6.3, the transient change of absorption obtained from the unannealed sample is compared to model calculations based on Eqns. 3-5. The calculated change of absorption (solid line) satisfactorily fits our optical data assuming $\xi = 8\ (\pm 1)*10^{-8}$ and $\sigma = 10\ (\pm 2)*10^{-9}\ cm^3 s^{-1}$. In order to demonstrate the significance of σ in our model calculation, the transient absorption change is also calculated for a lower capture rate as shown by the dotted line in Fig. 6.3.

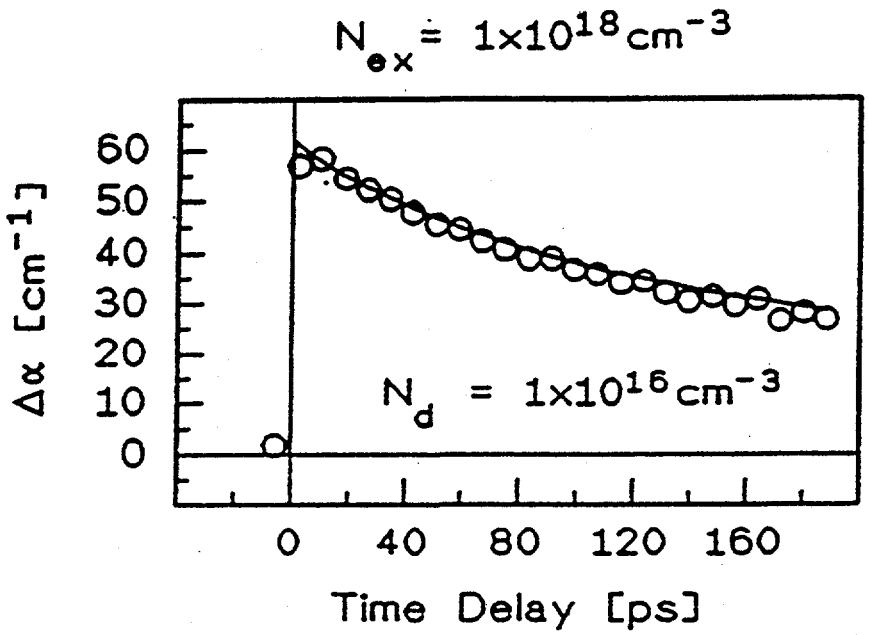

FIGURE 1

Transient change of absorption, $\Delta\alpha$, obtained from an annealed a-Si:H film (experimental data: open circles; model calculation: solid line)

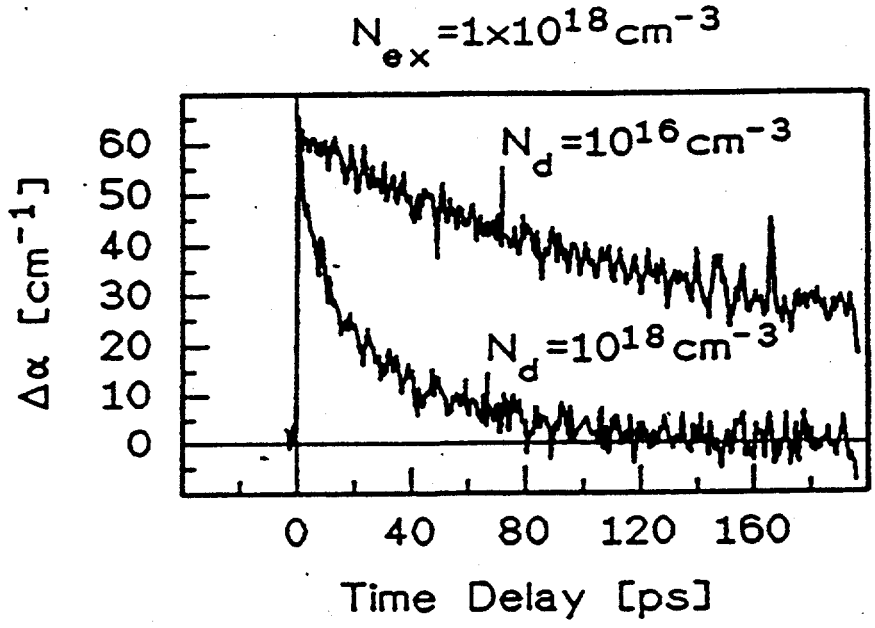

FIGURE 2

Transient change of absorption, $\Delta\alpha$, obtained from the low temperature deposited a-Si:H film before ($N_d \approx 10^{18}\ cm^{-3}$) and after annealing ($N_d \approx 10^{16} cm^{-3}$).

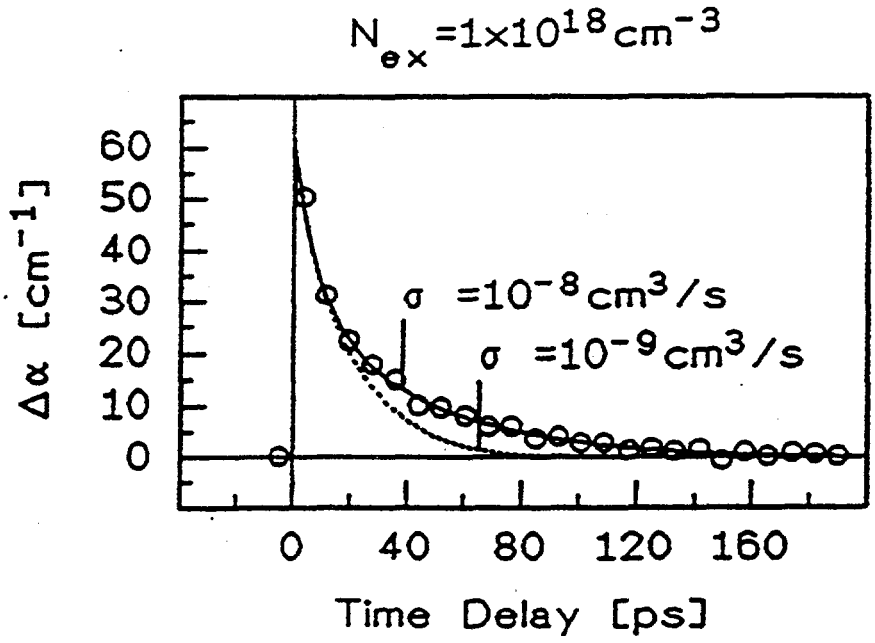

FIGURE 3

Transient change of absorption obtained from the defective a-Si:H compared to model calculation based on Eqns. 3-5 (see text).
(experimental data: open circles;
model calculation for $\sigma = 10^{-8}$ cm^3s^{-1}: solid line;
model calculation for $\sigma = 10^{-9}$ cm^3s^{-1}: dotted line).

The recovery of absorption in a-Si:H with a defect density, $N_d \approx 10^{18}$ cm^{-3}, is consistent with an ultrafast recombination process, rather than a deep trapping process. We propose an Auger-mechanism where recombining e-h pairs can ionize a dangling bond state (D^0). The ionized dangling bond state (D^+) is then neutralized by the capture of free electrons, also on a psec time scale.

REFERENCES

1. A. Esser, K. Seibert, H. Kurz, G. N. Parsons, C. Wang, B.N. Davidson, G. Lucovsky and R.J. Nemanich, Phys. Rev. **B41** (1990) 2879.

2. K. Hattori, H. Okamoto and Y. Hamakawa, Phil. Mag. **B75** (1988) 13.

3. G.N. Parsons, C. Wang, M.J. Williams and G. Lucovsky, Appl. Phys. Lett. **56** (1990) 1895.

4. J.A. Valdmanis and R.J. Fork, IEEE J. of Quantum Electronics, **QE-22** (1986) 122.

5. J. Strait and J. Tauc, Appl. Phys. Lett. **47** 589 (1985).

6. A. Hangleiter, Phys. Rev. **B37** (1988) 2594.

7. M. Stutzmann, W. B. Jackson, and C. C. Tsai, Phys. Rev. **B32** (1985) 23.

7. Modelling of Bond and Dihedral Angle Disorder in a-Si:H

We have applied a tight-binding model to Si-Bethe lattice structures in order to investigate the effects of bond-angle, and/or dihedral angle disorder. We have used a Hamiltonian with nearest and second-nearest neighbor interactions, and have been able to identify and separate the effects bond angle disorder and dihedral angle disorder on the states at the states at the conduction and valence band edges. We have systematically investigated the formation of electronic states in the region of the conduction and valence band edges of a-Si as functions of variations in the bond and dihedral angle distributions. Local Density of States (LDOS) for Si atoms in disordered environments have been calculated using the cluster Bethe lattice method with a tight-binding Hamiltonian containing both first and second nearest neighbor interaction terms. We conclude that the change in orbital overlap, incurred from rotations about the axes defining the dihedral angle distortions, is the origin of the effect of dihedral angle disorder on the electronic states near the band gap.

Short range disorder in a-Si can effect the electronic density of states (DOS) near the band edges, shift the band edges or create discrete states in the band gap.

This paper presents a study of short range disorder arising from bond angle distortions on the DOS of a-Si near the band edges. Raman scattering studies of a-Si and a-Ge by Lannin have related the bond angle disorder to a shift in the optical energy gap[1]. Previous studies using a tight-binding approach have shown valence band states for individual atoms in distorted tetrahedral environments[2,3] or have estimated the bounds for band tailing due to bond and dihedral angle distortions[3,4]. The Hamiltonians in these studies were restricted to nearest neighbor interactions, whereas our cal-culations have been performed with a tight-binding Hamiltonian that includes both first and second neighbor interaction terms.

We employ the Cluster-Bethe-Lattice (CBL) method which involves attaching an infinite Bethe lattice to the unsaturated bonds at the surface of a cluster. The Bethe lattice consists of an infinite network of 4-fold coordinated atoms with no ring structures, and provides an excellent boundary condition to the surface of the cluster, yielding a smooth, continuous energy eigenvalue spectrum for the DOS. This technique allows us to investigate local bond angle distortions or obtain an averaged DOS for an infinite network of distorted tetrahedra.

The LDOS of the i'th atom is related to the one electron Green's function by,

$$n_i(E) = -(1/\pi)\,\mathrm{Tr}\,(\,\mathrm{Im}\,g_{ii}(E)\,), \qquad (1)$$

where the Green's function, gii is determined by solving the coupled equations

$$(E\bullet I - H_{ii})g_{ij} = \delta_{ij} + \Sigma\, H_{i\lambda}g_{\lambda j}, \qquad (2)$$

and λ is summed over first and second neighbors. The self-consistent solution for an ideal or non-distorted Bethe lattice with second neighbor interactions terms has been published by Allen et al.[5] Effective Bethe lattice fields are then *attached* to the unsaturated or surface bonds of the distorted cluster that is being examined.

The Hamiltonian utilizes a tight-binding sp^3 orbital basis with first and second neighbor interactions as obtained by Pandey from a fit to the band structure of crystalline Si[6], done in the context of the two-center approximation[7]. Applied to an *ideal* Bethe lattice, these parameters yield a band gap of 2.2 eV. The cluster consists of 17 atoms: an atom surrounded by two shells of neighbors terminated by an infinite Bethe lattice. The second neighbor interaction terms in the Hamiltonian are scaled using a $1/r^2$ law to account for the changes in distances, Δr, to second neighbors with a cutoff distance of 4.47 Å (the approximate distance to the 3rd neighbor shell).

Before considering bond angle distortions in clusters with different dihedral

angles, we first identify the effects on the electronic LDOS near the band gap arising from rotations in the dihedral angle alone. The rotations involved in changing the dihedral angle do not distort any bond angles, but instead change third neighbor distances of the atoms (see Fig. 7.1). Only 1 rotation is shown, but rotations about the remaining 3 bonds coming from the center atom are done similarly.

In Fig. 7.2 we show the difference between the eclipsed and staggered configurations on the LDOS of the center atom for the case of rotating all the dihedral angles in order to retain the symmetry in the second neighbor shell of the center atom. All bond angles are *ideal*; i.e., = 109.47°. The dip at -0.6 eV represents a small shift of the valence band edge to lower energies, and the flat portion, from -0.5 eV to 1.7 eV, indicates no difference in band gap states for the two configurations. We have also studied the LDOS of other atoms in the cluster and observed larger changes in the LDOS, particularly in the conduction band. The magnitudes of the changes in the LDOS for the variations in dihedral angle are dependent on the cutoff distance and the scaling law, but nonetheless, the Hamiltonian must contain distance dependent interaction terms involving atoms beyond first neighbors to yield any difference between the staggered and eclipsed configurations.

We can now consider bond angle distortions of the center atom in the staggered and eclipsed configurations. For a disordered bond angle environment, we chose the configurations of the center atom consistent with the normal bond bending modes of the Td point group; the triply degenerate F mode and the doubly degenerate E mode shown in Fig. 7.3. The bond angle distortions for both modes correspond to 8° rotations, and yield a distorted tetrahedra whose six bond angles are 8° or less in magnitude from the ideal value of 109.47°.

The results for the change in the LDOS of the center atom for an E mode distortion for both staggered and eclipsed dihedral angle configurations are shown in Fig. 7.4. The most noticeable difference between the two geometries is at the top of the valence band. The eclipsed configuration does not show as much of an increase at the valence band edge as the staggered configuration. This can be under-stood by referring to Fig. 7.2 where the eclipsed configuration shows a decrease in states at the valence band edge, which *cancels out* some of the increase arising from the E mode distortion.

Previous calculations using the same Hamiltonian demonstrated that bond angle distortions can change the LDOS near the band edges and that these changes are enhanced by, but not dependent on, the appropriate scaling of the second neighbor terms in the Hamiltonian[8]. The basic features in the resulting LDOS arise from breaking the Td symmetry of the nearest neighbors which also can be adequately modeled using only nearest neighbor terms in the Hamiltonian. We have repeated the same calculation of the E mode distortion using a Hamiltonian with only first neighbor interactions of a five orbital sp^3s^* basis. This utilizes an additional s^* parameter to reproduce more accurate conduction band structure in crystalline Si[9]. The trends in the change in the LDOS due to the E mode bond angle distortions shown in Fig. 7.5 are found to be similar as those of the 2nd neighbor Hamiltonian, but the first neighbor Hamiltonian shows no difference in the LDOS changes between the staggered and eclipsed configurations. This demonstrates the importance of second neighbor interaction terms. In a Hamiltonian with only first neighbor interactions, some information relative to positions of second neighbors is *passed along* the Green's function through an intermediate atom. Therefore, changes in the states due to local bond angle distortions can still appear with the first neighbor terms, but since a dihedral angle rotation does not change the nearest neighbor symmetry, the nearest neighbor Hamiltonian is unable distinguish between the eclipsed and staggered configurations.

The results of the change in LDOS of the center atom in an F mode distortion in Fig. 7.6. This mode is more sensitive to dihedral angle variations than the E mode distortions. Calculations done with the nearest neighbor Hamiltonian on the F mode also showed no difference between the staggered and eclipsed configurations and resembled the curve for the staggered configuration as expected from the arguments given above.

Bond angle distortions and dihedral angle variations in clusters embedded in a Bethe lattice show effects on the LDOS at the top of the valence and at the bottom of the conduction band. Both E and F mode distortions increase the states at the edge of the conduction and valence band for the staggered configurations. Rotation of the dihedral angles to the eclipsed configurations can reduce the magnitude of states at the band edges by pushing these states farther into the band. This effect cannot be seen with a nearest neighbor Hamiltonian, which can model the bond angle distortions adequately, but cannot account for changes in distance and symmetry of

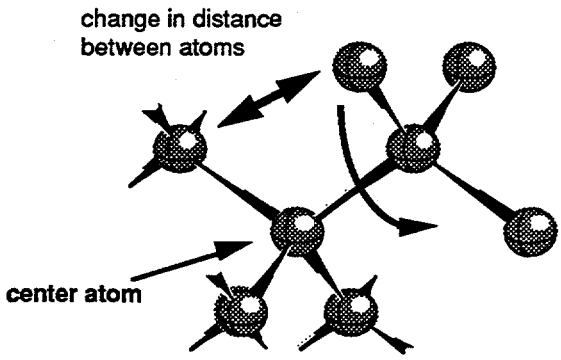

FIGURE 7.1
Dihedral angle rotation and the resultant change in distance between the atoms defining the dihedral angle.

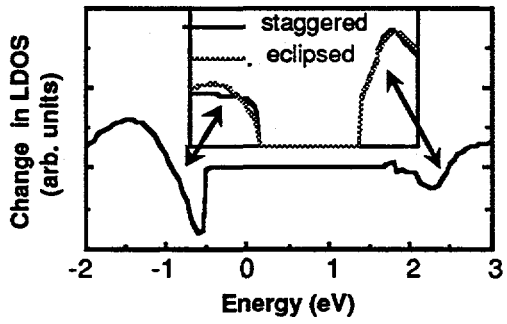

FIGURE 7.2
Difference in LDOS of the center atom for eclipsed and staggered configurations, with the staggered geometry as the reference state. The insert contains LDOS for the 2 configurations corresponding to the energy region shown in the plot.

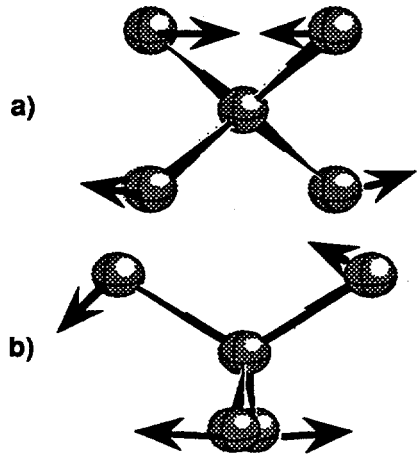

FIGURE 7.3
Distortions corresponding to normal vibrational modes of Td point group: (a) F mode distorts atoms in plane defined by its bond and the bond of another atom for a "scissors like" motion; and (b) E mode distorts atoms perpendicular to the same plane for a twisting motion.

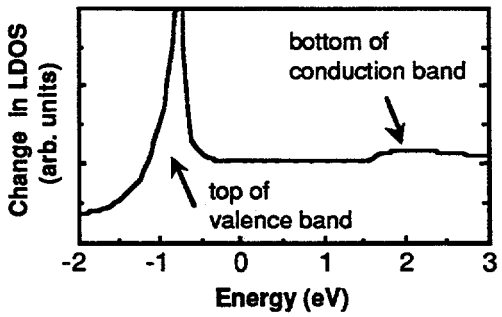

FIGURE 7.4
Change in LDOS near the band gap due to an E mode bond angle distortion as described in Fig.3 using nearest neighbor Hamiltonian, showing identical results for staggered and eclipsed configurations.

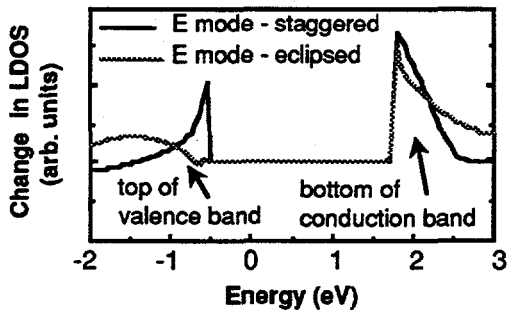

FIGURE 7.5
Change in LDOS near the band gap due to an E mode bond angle distortion for both staggered and eclipsed configurations. Sharp features at edges represent a shift of the edge into or away from the gap.

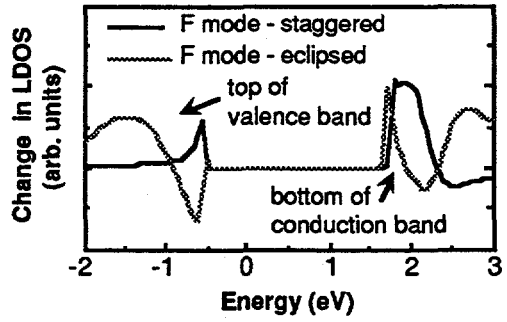

FIGURE 7.6
Change in LDOS near the band gap due to an F mode bond angle distortion for both staggered and eclipsed configurations. Sharp features at the edge represent a shift of the edge into or away from the gap.

the outer shells of atoms due to intermediate range disorder such as the dihedral angle variations. A key component of modeling the dihedral angle distortion are the 2nd neighbor interaction terms and the distance scaling law used with them. We are currently investigating other tight-binding parameters to determine the sensitivity of these results to the empirical fit of the terms and their relationship to neighbor distance on the band structure of Si.

REFERENCES

1. Lannin, J. S., in Physics of Disordered Materials, ed. by D. Adler, B.B. Schwarz and S.R. Ovshinsky (Plenum Press, NY, 1985) p.175.

2. J. D. Joannopoulos, Phys. Rev. **B 16** (1977) 2764.

3. B. N. Davidson and G. Lucovsky,. MRS Symp. Proc. **192** (1990) 279.

4. J. Singh, Phys. Rev. **B 23** (1981) 4156.

5. D. C. Allan, J. D. Joannopoulos and W. B. Pollard, Phys. Rev. **B 25** (1982) 1065.

6. K. C. Pandey and J. C. Phillips, Phys. Rev. B**13** (1976) 750.

7. J. C. Slater and G. F. Koster, Phys. Rev. **94** (1954) 1498.

8. B. N. Davidson, G. Lucovsky and J. Bernholc, MRS Symp. **219** (1991), in print.

9. P. Vogl, H. Pl. Hjalmarson, and J. D. Dow, J. Phys. Chem. Solids **44** (1983) 365.

8. Chemical Effects in Local Bonding Arrangements in a-Si:H: Ab Initio and Empirical Calculations

We have used ab initio and empirical calculations to study non-random bonding arrangements in a-Si,O:H and doped a-Si:H films. The two approaches give comparable results for the bond energies of SiH groups that are near-neighbors to the oxygen and dopant atoms. The calculations have been used to develop a model for the way in which these bonding arrangements are created in thin film deposition processes in which surface, rather than gas phase reactions dominate; i.e., for the range of deposition parameters used to produce electronic or device grade materials.

We have identified several important *non-statistical* bonding environments in alloyed and doped a-Si:H. These include O-Si-H *linkages* in a-Si,O:H alloys, and P^{+}-Si-H and Si-B^{-}-H *linkages* that play a significant role in the doping processes in a-Si:H. We present the experimental evidence for these bonding arrangements, and a model that accounts for their creation during film deposition.

There have been many studies of the bonding of hydrogen in a-Si alloys and in doped a-Si:H. IR absorption is an important technique for studying alloys when the densities of H- and alloy-atoms are greater than a few atomic percent, and has been applied to a-Si:H with O, N, Ge, C, B, P and As as alloy constituents[1]. NMR has been used to study P and B dopant atoms for concentrations <1 at.% [2]. Local atomic arrangements of Si, O and H in a-Si,O:H have been studied by IR for bonded-H concentrations, [H], of ~10-15 at.%, and bonded [O] levels between ~1 and 20 at%. These concentrations of H do not promote significant polyhydride formation so that the local bonding of H-atoms is restricted to SiH groups. The data also indicate no detectable incorporation of Si-OH groups, consistent with other studies that show the OH can be incorporated in a-SiO_2 thin films, but not in a-SiO_x:H for $x < 2$ [3]. Analysis of spectral data for SiH vibrations for low [O] indicates two bonding arrangements: i) one with 3 Si-atoms back-bonded to the Si-atom of the SiH group; and ii) one with one of the Si-atoms replaced by an O-atom (see Fig. 8.1). These two arrangements are distinguished by their IR absorptions: stretching and bending modes at 2000 cm^{-1} and 630 cm^{-1} in the first case, and ~2100 cm^{-1} and 780 cm^{-1} in the second. This second set of absorptions scales with [O] for a fixed [H][3], and this indicates a *non-statistical* occurrence of the O-Si-H linkage. In a random covalent network of Si, O and H-atoms with each atom bonded according to its valence of 4, 2 and 1, respectively, the absorption at 780 cm^{-1} would not scale linearly with the oxygen con-centration over the range of [O] reported.

The local bonding arrangements of H--atoms in doped a-Si:H can not be detected by IR, but have been identified through an analysis of NMR data [2]. These data indicate: i) for P-doped a-Si:H, H-atoms are second neighbors to the fourfold-coordinated and positively charged P-donors; and ii) for B-doped a-Si:H, H-atoms are bonded directly to the fourfold-coordinated, negatively charged B-acceptors, with the other three B-bonds being to Si-atoms; see Fig. 8.1. For each of the three bonding arrangements, shown in Fig. 8.1, that include Si- and H-atoms, and either O, or P or B, there is an *unexpected*, and non-statistical occurrence of these groups. This implies a chemical driving force that promotes their creation. In addition, electrically *inactive*, threefold-coordinated P- and B- atoms are also present in the doped materials [5].

Bond energies have been determined in two ways for 3 bonding configurations that include Si, O and H: 3Si-SiH, 2Si,O-SiH and 3O-SiH. This was done: i) using

empirical relationships based on differences in electronegativities[4]; and ii) by ab-initio calculations[6] applied to hydrogen-terminated clusters that contain the SiH group, but with different numbers of Si- and O-atoms back-bonded to the Si-atom of that group.

The calculated Si-H energies are given below:

Group	Bond Energy (eV)	Relative Energy
	Ab-initio Calculation	
3Si-SiH	4.06	1.00
2Si,O-SiH	4.21	1.04
3O-SiH	4.66	1.15
	Empirical Calculation	
3Si-SiH	3.92	1.00
2Si,O-SiH	4.14	1.06
3O-SiH	4.64	1.18

The bond-energies, normalized to 3Si-SiH, demonstrate that both approaches yield similar relative bond-energies for the three groups. In addition, both calculations give differences in the IR frequencies for the Si-H bond-stretching modes that are in agreement with each other, and with experiment: about +90 to +100 cm^{-1} for each substituted O-atom.

Ab-initio calculations have not as yet been performed on clusters that include the charged and electrically active P^+ and B^- dopant atoms. We have estimated bond energies for these configurations using the empirical approach based on electronegativities[4]. We first compute bond energies for some of the probable bonding arrangements involving H-atoms, and then for the case of the P-atom bonding environments establish a *chemical equivalence* between the O-Si-H and P^+-Si-H *linkages* through a calculation of the *partial charge* on the Si and H atoms. The empirically determined bond energies are given below:

Group	Bond Energy (eV)	Relative Energy
2Si,P^+-SiH	4.37	1.00
2Si-PH	4.18	0.96
3Si,B^--H	4.56	1.00
2Si-BH	4.99	1.09

The calculation of partial charges below establishes a *linkage* between these empirical bond energy calculations, and the ab-initio and empirical calculations presented above:

Bonding Group	Si Charge	H Charge
3Si-SiH	+ 0.04 e	- 0.15 e
2Si,O-SiH	+ 0.15 e	- 0.05 e
2Si,P^+-SiH	+ 0.19 e	- 0.02 e

Partial charges obtained from ab-initio calcu-lations give equivalent trends for the first two groups. The partial charges on the Si- and H-atoms for the 2Si,O-SiH and 2Si,P^+-SiH groups are similar, and therefore exhibit *equivalent* differences with respect to the corresponding partial charges of the 3Si-SiH group. In the spirit of the empirical models, this implies comparable bond energies for these SiH groups, and therefore similar differences with respect to bond energy of the SiH group in the 3Si-SiH cluster. This is supported by the bond energies calculations that we have presented above.

The questions that we address in this paper relate to the chemical effects that promote the non-statistical or non-random bonding groups that have been identified experimentally -- 2Si,O-SiH, 2Si,P^+-SiH and 3Si,B^--H. Consider first 2Si,O-SiH: these groups are present in a-Si,O:H alloys formed by several techniques, including Remote PECVD, where homo-geneous reactions between Si- and O-atom precursors do not readily occur. In point of fact, there is no mass spectroscopic evidence to indicate that precursors with Si-O groups, such as silanols or siloxanes, are formed by gas phase reactions between SiH_4, and O-containing molecules such as O_2 and N_2O. This means that the O-Si-H arrangements are *created* at the growth surface during film deposition.

a-Si,O:H alloys are typically deposited at temperatures between 225 and 300°C. Film growth proceeds from a heavily hydrogenated surface, so that differences in the bonded H-concentrations derive from the rate at which H atoms are thermally *removed* from that growth surface. Since bond energies of all relevant SiH groups are of the order of 4 eV, the relatively small differences between these bond-energies, ~0.2 eV, for SiH in 3Si-SiH, and in 2Si,O-SiH clusters cannot completely account for the preferential retention of H in 2Si,O-SiH arrangements.

It has been shown that H-atoms initially bonded to a crystalline Si surface, can be removed from that surface at low temperatures by exposure to atomic hydrogen. This is followed by some type of surface reconstruction, as in the transition from a dihydride H-terminated Si(100) surface with 1x1 symmetry to an SiH-terminated surface with a 2x1 symmetry: surface dihydride groups are converted to monohydride groups, and a Si-Si dimer bond is formed.

We propose that plasma generated H-atoms (or protons) play a similar role in H-removal from hydrogen-terminated a-Si surfaces during film deposition. The rate limiting step for a surface reaction is often through the creation of an intermediate arrangement in which the Si surface atom is over-coordinated as in 3Si-Si-2H. This surface structure is energetically unstable with respect to interaction with an SiH_3 group through a reaction of the following form:

$$3Si\text{-}Si\text{-}2H + SiH_3 \rightarrow 3Si\text{-}Si\text{-}SiH_3 + H_2 \qquad (1)$$

The rate of attachment of H, that creates the over-coordination will depend on the partial charge on the Si atom, and whether the H that is to be attached is an atom or a proton. If we assume that protons are the active species, then the rate of attachment is expected to decrease as the partial charge on the Si atom of the surface bonding group increases and becomes more positive. This factor could account for the increased stability of the bonding arrangements involving O and P^+ atoms. However, if the active species is a H-atom (a hydrogen radical) then the rate of attachment could be independent of the partial charge on the Si-atom. However, the groups with O and P^+ would still be retained if the active species were H-radicals, since the break-up reaction for the release of additional hydrogen atoms would favor the retention of both the 2Si,O-SiH and 2Si,P^+-SiH groups, due to their higher SiH bonding energies with respect to 3Si-SiH. The energy differences between SiH bonds in the *favored* groups are 0.2 and 0.37 eV, respectively, and are sufficient to account for preferential formation. Thus, the majority of the H-rejection from the growth surface must involve surface 3Si-SiH groups. In a complementary way, the same types of surface reaction chemistry also favor a preferential retention of 2Si,B^--H configurations with respect to t3Si-SiH groups; this is due to the large difference in energy between SiH and B^--H.

Based on the experimental studies of a-Si,O:H, and P and B-doped a-Si:H, there are local bonding environments involving Si and H atoms with either O, P or B atoms that are non-statistical in the sense that they would not be anticipated solely by the relative concentrations of these atoms in the films. This infers that there are

chemical driving forces for their creation in the deposited films. Since SiH groups, as well as OH, PH and BH groups all have bonding energies of about 4 eV, small differences in these energies by themselves cannot account for preferential formation of SiH or B-H bonding groups for films deposited at 200-300°C. This leads us to propose a mechanism for the occurrence of the non-statistical bonding arrangements that is related to surface reaction chemistry. The model includes three steps: i) the formation of an intermediate structure in which the Si, and/or B or P atoms are over-coordinated by additional H-atoms; ii) the break-up of these surface intermediates through the release of molecular H - H_2; and iii) the attachment of an SiH_n group that continues the film growth process. In addition to these bonding sites involving H atoms and the dopant atoms P and B, there are other bonding groups in which P and B are threefold-coordinated and inactive with respect to doping. In this context, the calculated relative bonding energies for the *doping and inactive groups* are in accord the observation that the doping efficiency for P-atoms is significantly higher than for B-atoms[5].

REFERENCES

1. G. Lucovsky and W.B. Pollard, in *The Physics of Hydrogenated Amorphous Silicon II*, ed. by J.D. Joannopoulos and G. Lucovsky (Springer-Verlag, Berlin, 1984), p. 301.

2. J.B. Boyce, S.E. Ready and C.C. Tsai, J. Non-Cryst. Solids **97 & 98** (1987) 345.

3. G. Lucovsky, S.S. Chao, J.E. Tyler and W. Czubatyj, Phys. Rev. **B28** (1983) 3225.

4. R.T. Sanderson, Chemical Bonds and Bond Energy (Academic Press, New York, 1971).

5. W.E. Spear and P.G. LeComber, Phil. Mag **33** (1976) 935.

6. Z. Jing and J.L. Whitten, Phys. Rev. **B44** (1991) 1741.

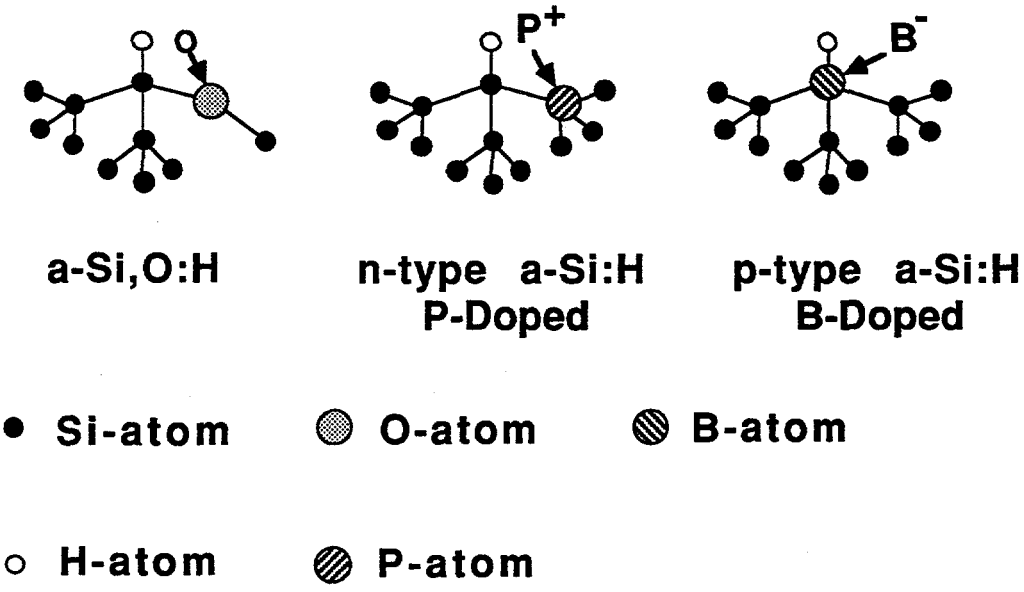

Figure 8.1
Local bonding arrangements of H-atoms in
a-Si,O:H, a-Si:H (n-type) and a-Si:H(p-type)

II. Research Publications and Presentations

A. Papers Published

1. M.J. Williams, G.N. Parsons, C. Wang and G. Lucovsky, "Deposition of Electronic-Grade Amorphous Silicon: Induced Defect Relaxation", Proceedings of the Twentieth International Conference on the Physics of Semiconductors, 1990.

1. B. N. Davidson and G. Lucovsky, "Electronic states in the gap of a-Si from bond angle variations.", MRS Symp. Proc. **192**, 279 (1990).

2. B. N. Davidson, G. N. Parsons, C. Wang and G. Lucovsky, "Polyhydride bonding groups in PECVD amorphous Si thin films.", Mat. Res. Soc. Symp. Proc. **165**, 209 (1990).

3. C. Wang, G.N. Parsons, E.C. Buehler, R.J. Nemanich and G. Lucovsky, Formation of Microcrystalline Silicon Films by Reactive Magnetron Sputtering (RMS) Process", MRS Symp. Proc. **164**, 21 (1990).

4. G.N. Parsons, C. Wang and G. Lucovsky, "Annealing of "Intrinsic" and Photo-induced Defects in a-Si:H Thin Films", Proceeding of 17th International Conference on Metallurgical Coatings and 8th International Conference on Thin Films (1991).

5. G. N. Parsons and G. Lucovsky, "Nitrogen Incorporation In a-Si,N:H Alloy Films Produced by Remote PECVD, MRS Symp. Proc. **165**, 85 (1990).

6. C. Wang, G.N. Parsons and G. Lucovsky. "Microcrystalline Silicon thin Film Deposited by Reactive Magnetron Sputtering and Remote Plasma enhanced Chemical Vapor Deposition Process", MRS Symp. Proc. **192**, 535 (1990).

7. G.N. Parsons, C. Wang and G. Lucovsky. "Reduction of Electronic Defects by Annealing in Hydrogenated and Unhydrogenated Amorphous Silicon", MRS Symp. Proc. **192** (1990).

8. S.S. Kim, C. Wang, G.N. Parsons and G. Lucovsky. "a-Si:H Thin Film Transistors and Logic Circuits Fabricated in an Integrated Multichamber System", MRS Symp. Proc. **192**, 775 (1990).

9. C. Wang and G. Lucovsky, "Intrinsic Microcrystalline Silicon Deposited by Remote PECVD: A New Thin Film Photovoltaic Material", Proceeding of 21st IEEE Photovoltaic Specialists Conference.

10. C. Wang, C.H Bjorkman, D.R. Lee, M.J. Williams and G. Lucovsky, "Deposition of Heavily Doped μc-Si Films by Remote PECVD Process", MRS Symp. Proc. **204**, 227 (1990).

11. D. R. Lee, C. H. Bjorkman, C. Wang, and G. Lucovsky, "Studies of MOS and Heterojunction Devices Using Doped μc-Si and a-Si," MRS Symp. Proc. **219**, 395 (1991).

12. C. Wang, M.J. Williams and G. Lucovsky, "Preparation of Microcrystalline Silicon Thin Films by Remote PECVD", J. Vac. Sci. Technol. **A3**, 444 (1991).

13. C. Wang, G. Lucovsky and R.J. Nemanich, "Deposition of the Amorphous and Microcrystalline Si,C Alloy Films by Remote PECVD Process", MRS Symp. Proc. **219**, 751 (1991).

14. M.J. Williams, C. Wang, and G. Lucovsky, "Deposition and Characterization of Near "Intrinsic" μc-Si Films Deposited by Remote Plasma Enhanced Chemical Vapor Deposition", MRS Symp. Proc. **219**, 389 (1991).

15. G. Lucovsky and C. Wang, "Barrier Limited Transport Mechanisms in Doped μc-Si and μc-Si,C", MRS Symp. Proc. **219**, (1991).

16. B. N. Davidson, G. Lucovsky, and J. Bernholc, "Effect of the Local Disorder in a-Si on the Electronic Density of States at the Band Edges", MRS Symp. Proc. **219**, (1991).

17. G. Lucovsky, C. Wang, R.J. Nemanich and M.J. Williams, "Deposition of μc-Si and μc-Si,C Thin Films by Remote Plasma-Enhanced Chemical-Vapor Depositon", Solar Cells **30**, 419 (1991).

B. Presentations at Technical Meetings

1. C. Wang, C.H Bjorkman, D.R. Lee, M.J. Williams and G. Lucovsky, "Deposition of Heavily Doped μc-Si Films by Remote PECVD Process", MRS Fall Meeting, Boston, MA, November, 1990.

2. M.J. Williams, Cheng Wang, and G. Lucovsky, "Microcrystalline Silicon Deposited by Remote Plasma Enhanced Chemical Vapor Deposition", International Conference on Stability of Amorphous Silicon Materials and Solar Cells Denver, CO., February 20-22, 1991.

3. M.J. Williams, C. Wang, and G. Lucovsky, "Deposition and Characterization of Near "Intrinsic" μc-Si Films Deposited by Remote Plasma Enhanced Chemical Vapor Deposition", MRS Spring Meeting, Anaheim, CA., April 1991.

4. M.J. Williams, Cheng Wang, and G. Lucovsky, "Photoconductivity and Optical Stability of Intrinsic μc-Si Films Formed by Remote Plasma Enhanced Chemical Vapor Deposition, Remote PECVD", 14th ICAS, Garmisch-Partenkirchen, FRG, August 1991.

5. D. R. Lee, C. H. Bjorkman, C. Wang, and G. Lucovsky, "Studies of MOS and Heterojunction Devices Using Doped μc-Si and a-Si," MRS Spring Meeting, Anaheim, CA., April 1991.

6. D. R. Lee, C. H. Bjorkman, and G. Lucovsky, "Effective Electron Affinities in Doped a-Si:H and μc-Si Films as Determined from Studies of MOS Capacitors", 14th ICAS, Garmisch-Partenkirchen, FRG, August 1991.

7. C. Wang, G. Lucovsky and R.J. Nemanich, "Deposition of the Amorphous and Microcrystalline Si,C Alloy Films by Remote PECVD Process", MRS Spring Meeting, Anaheim, CA., April 1991.

8. C. Wang, G. Lucovsky and R.J. Nemanich, "Preparation and Properties of Dopeda-Si,C:H and μc-Si,C Alloy Films by Remote PECVD", 14th ICAS, Garmisch-Partenkirchen, FRG, August 1991.

9. B. N. Davidson, G. Lucovsky, and J. Bernholc, "Effect of the Local Disorder in a-Si on the Electronic Density of States Near the Band Gap", APS March Meeting, Cincinnati, OH, March 1991.

10. B. N. Davidson, G. Lucovsky, and J. Bernholc, "Effect of the Local Disorder in a-Si on the Electronic Density of States at the Band Edges", MRS Spring Meeting, Anaheim, CA., April 1991.

12. B. N. Davidson, G. Lucovsky, and J. Bernholc, "Effect of the Local Disorder in a-Si on the Electronic Density of States Near the Band Edges", 14th ICAS, Garmisch-Partenkirchen, FRG, August 1991.

13. G. Lucovsky, C. Wang, R.J. Nemanich and M.J. Williams, "Deposition of μc-Si and μc-Si,C Thin Films by Remote Plasma-Enhanced Chemical-Vapor Depositon", 10th PV Research and Development Meeting, Lakewood, CO, Octorber 1991.

14. G. Lucovsky and C. Wang, "Barrier Limited Transport Mechanisms in Doped μc-Si and μc-Si,C", MRS Spring Meeting, Anaheim, CA., April 1991.

15. G. Lucovsky, Z. Jing and J.L. Whitten, "Chemical Induction Effects: O-incorporation in, and Substitutional Doping of a-Si:H", 14th ICAS, Garmisch-Partenkirchen, FRG, August 1991.

16. A. Esser, H. Heesel, H.Kurz, C. Wang, M.J. Williams and G. Lucovsky, "The Role fo Dangling Bond States in the Picosecond Recovery of Photoinduced Absorption in a-Si:H", 14th ICAS, Garmisch-Partenkirchen, FRG, August 1991.

c. Papers Accepted for Publication

1. M.J. Williams, Cheng Wang, and G. Lucovsky, "Microcrystalline Silicon Deposited by Remote Plasma Enhanced Chemical Vapor Deposition", AIP Conference Proceedings **234**, (1991).

2. D. R. Lee, C. H. Bjorkman, and G. Lucovsky, "Effective Electron Affinities in Doped a-Si:H and μc-Si Films as Determined from Studies of MOS Capacitors," J. of Non-Cryst. Solids (1991).

3. B. N. Davidson, G. Lucovsky, and J. Bernholc, "Effect of the Local Disorder in a-Si on the Electronic Density of States Near the Band Edges", J. of Non-Cryst. Solids (1991).

4. G. Lucovsky, Z. Jing and J.L. Whitten, "Chemical Induction Effects: O-incorporation in, and Substitutional Doping of a-Si:H", J. of Non-Cryst. Solids (1991).

5. A. Esser, H. Heesel, H.Kurz, C. Wang, M.J. Williams and G. Lucovsky, "The Role fo Dangling Bond States in the Picosecond Recovery of Photoinduced Absorption in a-Si:H", J. of Non-Cryst. Solids (1991).

6. C. Wang, G. Lucovsky and R.J. Nemanich, "Preparation and Properties of Dopeda-Si,C:H and μc-Si,C Alloy Films by Remote PECVD", J. of Non-Cryst. Solids (1991).

7. M.J. Williams, Cheng Wang, and G. Lucovsky, "Photoconductivity and Optical Stability of Intrinsic μc-Si Films Formed by Remote Plasma Enhanced Chemical Vapor Deposition, Remote PECVD", J. of Non-Cryst. Solids (1991).

d. Talks and Posters Accepted for Publication

1. J. A. Theil, and G. Lucovsky, "Relation of Precursors in the N_2/SiH_4, and NH_3/SiH_4 Gas Systems to Growth of Silicon Nitride at Low Temperatures by Remote Plasma Enhanced Chemical Vapor Deposition", 38th AVS National Symposium, Seatle, WA, November 1991.

2. D. R. Lee, Yi Ma, T. Yasuda, C.H. Bjorkman, and G. Lucovsky, "Stacked Gates with Doped μc-Si Electrodes and SiO_2 Dielectrics, Both Deposited by Remote PECVD," 38th AVS National Symposium, Seatle, WA, November 1991.

Document Control Page	1. NREL Report No. NREL/TP-451-4852	2. NTIS Accession No. DE92010560	3. Recipient's Accession No.

4. Title and Subtitle

Fundamental Studies of Defect Generation in Amorphous Silicon Alloys Grown by Remote Plasma-Enhanced Chemical-Vapor Deposition (Remote PECVD)

5. Publication Date

January 1993

6.

7. Author(s)

G. Lucovsky, R.J. Nemanich, J. Bernholc, J. Whitten, C. Wang, B. Davidson, M. Williams, D. Lee, C. Bjorkman, Z. Jing

8. Performing Organization Rept. No.

9. Performing Organization Name and Address

North Carolina State University
Departments of Physics and Materials Science and Engineering
Raleigh, North Carolina 27695-8202

10. Project/Task/Work Unit No.

PV221103

11. Contract (C) or Grant (G) No.

(C) XM-9-18141-2

(G)

12. Sponsoring Organization Name and Address

National Renewable Energy Laboratory
1617 Cole Blvd.
Golden, CO 80401-3393

13. Type of Report & Period Covered

Technical Report
1 September 1990 - 31 August 1991

14.

15. Supplementary Notes

NREL technical monitor: J. Benner

16. Abstract (Limit: 200 words)

This report describes major research accomplishments during Phase II of this subcontract. (1) We demonstrated that the remote PECVD process can be used to deposit heavily doped n-type and p-type a-Si:H thin films. (2) We optimized conditions for depositing undoped, near-intrinsic and heavily doped thin films of μc-Si by remote PECVD. (3) We extended the remote PECVD process to the deposition of undoped and doped a-Si,C:H and μc-Si,C alloy films. (4) We analyzed transport data for the dark conductivity in undoped and doped a-Si:H, a-Si,C:H, μc-Si and μc-Si,C films. (5) We studied the properties of doped a-Si:H and μc-Si in MOS capacitors using ~10 Ω-cm p-type crystalline substrates and thermally grown SiO_2 dielectric layers. (6) We collaborated with a group at RWTH in Aachen, Germany, and studied the contributions of process-induced defect states to the recombination of photogenerated electron pairs. (7) We applied a tight-binding model to Si-Bethe lattice structures to investigate the effects of bond angle, and dihedral angle disorder. (8) We used ab initio and empirical calculations to study non-random bonding arrangements in a-Si,O:H and doped a-Si:H films.

17. Document Analysis

a. Descriptors

amorphous silicon ; alloys ; PECVD deposition ; photovoltaics ; solar cells

b. Identifiers/Open-Ended Terms

c. UC Categories

271

18. Availability Statement

National Technical Information Service
U.S. Department of Commerce
5285 Port Royal Road
Springfield, VA 22161

19. No. of Pages

58

20. Price

A04